Identification of Protein Interactors of Cholesteryl Esters

A Thesis

submitted to

Indian Institute of Science Education and Research Pune in partial fulfilment of the requirements for the BS-MS Dual Degree Programme

by

Chaitanya Katkar

Indian Institute of Science Education and Research Pune

Dr. Homi Bhabha Road,

Pashan, Pune 411008, INDIA.

Date: 15th March, 2024

Under the guidance of

Supervisor: **Dr. Siddhesh Kamat**,

Associate Professor, Department of Biology,

Indian Institute of Science Education and Research Pune

From May 2023 to Mar 2024

INDIAN INSTITUTE OF SCIENCE EDUCATION AND RESEARCH PUNE

Certificate

This is to certify that this dissertation entitled "**Identification of Protein Interactors of Cholesteryl Esters**" towards the partial fulfilment of the BS-MS dual degree programme at the Indian Institute of Science Education and Research, Pune represents study/work carried out by Chaitanya Katkar at Indian Institute of Science Education and Research under the supervision of Dr. Siddhesh Kamat, Associate Professor, Department of Biology, during the academic year 2023-2024.

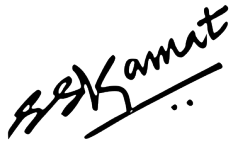

Dr. Siddhesh Kamat

Committee:

Supervisor: Dr. Siddhesh Kamat

TAC: Dr. Harinath Chakrapani

This thesis is dedicated to my parents

Mr. Anand Katkar and Mrs. Archana Katkar

Declaration

I hereby declare that the matter embodied in the report entitled "**Identification of Protein Interactors of Cholesteryl Esters**" are the results of the work carried out by me at the Department of Biology, Indian Institute of Science Education & Research (IISER) Pune, under the supervision of Dr. Siddhesh Kamat, and the same has not been submitted elsewhere for any other degree. Wherever others contribute, every effort is made to indicate this clearly, with due reference to the literature and acknowledgement of collaborative research and discussions.

Chaitanya Katkar

Reg. No. 20191198

Table of Contents

List of Figures

Main

Supplementary

List of Abbreviations

CPDA	Cholesteryl Palmitate Diazirine Alkyne
ChDA	Cholesterol Diazirine Alkyne
PADA	Palmitic Acid Diazirine Alkyne
MβCD	Methyl-beta-cyclodextrin
CuAAC	Copper-catalysed Azide–Alkyne Cycloaddition
ReDiMe	Reductive Dimethylation
LC-ESI-QTOF-MS/MS	Liquid Chromatography coupled Electrospray Ionisation-Quadrapole-Time of Flight-Mass Spectrometry

Abstract

Cholesterol and cholesteryl esters form the major sterol component of an animal cell. While there are extensive studies on understanding protein-cholesterol interactions, the protein interactors of cholesteryl esters mostly remain unknown. Therefore, the possible signalling mechanisms for these biomolecules are largely elusive. In this study, we present a chemoproteomic strategy to identify the interactors of cholesteryl esters on a proteome-wide scale. For this purpose, we employ a photoreactive bioorthogonal cholesteryl ester probe to map these interactors. Our results demonstrate two ways to effectively deliver the cholesteryl ester probe into different cell lines, which enables analysis of these lipid-protein interactions. We also show a difference in these interactions in different cell lines, thus hinting at possibilities of identifying different protein interactors in different cells. Moreover, our microscopy data demonstrates that these interactions occur at a pan-cellular level and are not restricted to the plasma membrane. Lastly, the proteomics analyses could identify initial hits of proteins in the N2a cell line with both the probes. Taken together, we establish methods to study cholesteryl ester-protein interactome, which will enable identification of possible signalling roles of cholesteryl esters in the future.

Acknowledgments

I am truly grateful to the following individuals for their invaluable contributions in bringing out the best in me and helping me develop this thesis successfully.

First and foremost, I am deeply indebted to Dr. Siddhesh Kamat for his unwavering support and invaluable guidance throughout the project. Thank you so much, Dr. Siddhesh, for standing by me when my proteomics did not (!). Your ability to remain calm and troubleshoot problems even in absolutely chaotic situations is unparalleled and worth learning. Thank you for giving me this opportunity to understand chemical biology and thus work on such an interdisciplinary project, enhancing my knowledge both in Biology and Chemistry. I would also like to thank Dr. Harinath Chakrapani for his suggestions and feedback, which helped me better investigate the project.

I am grateful to Aakash Chandramouli for his exceptional guidance throughout the project. Thank you, Aakash, for being an amazing mentor and teaching me the required skills and techniques. Your knowledge of mass spectrometry and your understanding of biochemical tools is remarkable, and this has truly helped me push this project ahead. Thank you, Karthik and Ojal, for sharing your expertise in proteomics, without which the proteomics part of my project would have not been possible. I would like to thank Kamat lab members: Sonali, Kaveri, Arnab, Kundan, Kavita, Pooja, Abhishek, Neeraj, Maya, Archit and Sreedev for keeping a friendly and energetic lab atmosphere. My time at Kamat Lab has truly developed me both personally and professionally.

I would like to acknowledge Aakash for his help in the initial parts of the project (optimising the CPDA probe in DMSO), where we collectively worked to obtain the data. The chemical probes used in the study were synthesized by Dr. Kavita Sharma and Pooja Thakral, without which none of these studies would have been possible.

Lastly, I would like to thank my family and friends for their unconditional support and constant motivation, and IISER Pune for providing state-of-the-art facilities (especially the mass spectrometry and microscopy facility) and an amazing campus life. Each of these have played a significant role in determining the project's success.

Contributions

Contributor name	Contributor role
Dr. Siddhesh Kamat, Aakash Chandramouli, Chaitanya Katkar	Conceptualization Ideas
Dr. Siddhesh Kamat, Aakash Chandramouli, Karthik Shanbhag	Methodology
-	Software
Chaitanya Katkar	Validation
Dr. Siddhesh Kamat, Aakash Chandramouli, Chaitanya Katkar	Formal analysis
Chaitanya Katkar, Aakash Chandramouli	Investigation
Dr. Siddhesh Kamat	Resources
Chaitanya Katkar	Data Curation
Chaitanya Katkar	Writing - original draft preparation
Dr. Siddhesh Kamat, Aakash Chandramouli, Chaitanya Katkar	Writing - review and editing
Chaitanya Katkar	Visualization
Dr. Siddhesh Kamat, Aakash Chandramouli	Supervision
Chaitanya Katkar	Project administration
Dr. Siddhesh Kamat	Funding acquisition

This contributor syntax is based on the Journal of Cell Science CRediT Taxonomy[1].

[1] https://journals.biologists.com/jcs/pages/author-contributions

Chapter 1 Introduction

1.1 **Lipid-Protein interactions: an emerging field in cellular signalling**

Lipids are an important class of macromolecules that perform crucial roles in cells and thereby support the existence of nearly all life forms on Earth. The most well-studied function of lipids is their ability to form membranous structures that allow separation of the internal milieu of the cell from the external environment by acting as a barrier to the passage of polar molecules and ions (Alberts *et al.*, 2002). These membranous structures are formed by the self-assembly of amphipathic lipid molecules, which, depending on the nature of the lipids involved, can form micelles, vesicles, or planar bilayers (Dowhan and Bogdanov, 2002; Deamer, 2017). This feature also allows for compartmentalisation within the cells, a classic eukaryote feature. In addition, lipids are also well-known to be important for cellular bioenergetics as they are the reserve pool of energy (Allen, 1976). The cell can catabolize the storage lipids, usually through the β-oxidation pathway, and generate huge amounts of energy when needed (Schulz, 1991; Mannaerts *et al.*, 2000).

However, in addition to these extensively studied functions, lipids are also becoming known for serving as important signalling molecules, both as intracellular messengers as well as for inter-organ cross-talk (Sunshine and Iruela-Arispe, 2017). Signalling lipids bind to specific proteins and can modulate their activity, thereby mediating signal transduction inside and outside cells. For example, phosphatidylinositol 4,5-bisphosphate, which is present on the cytoplasmic face of the plasma membrane, is known to recruit and activate supramolecular protein complexes having specific structural motifs (called the PH and PX domains). This interaction serves as an important point of nucleation for initiating the formation of multienzyme complexes at the membrane, thus enabling the execution of crucial functions like exocytosis, endocytosis, membrane fusion, and phagocytosis in the cell. Moreover, phosphatidylinositol 4,5-bisphosphate is also known for providing anchorage to certain cytoskeletal proteins (Martin, 2012). Furthermore, upon stimulation by an external cue, phosphatidylinositol 4,5-bisphosphate is broken down into Inositol 1,4,5-trisphosphate

(IP3) and diacylglycerol (DAG), which are well-known for performing signalling roles in the cell by activating several proteins downstream (Martin, 2012; Katan & Cockcroft, 2020). Apart from inositol phospholipids, ceramides and sphingomyelin are also known for regulating the function of protein kinases and modulating important processes like cell division, differentiation, and migration (Pp, 2001; Stith et al., 2019). Further, they are also important mediators for inducing apoptosis, which is one of the protective strategies of most cells against cancer (Bieberich, 2008). To list a few more, Arachidonic acid (AA) signalling is known to be important in cardiovascular and cancer biology, and AA is also converted to other bioactive molecules (prostaglandins, thromboxanes, and leukotrienes), mediating diverse physiological processes downstream (Tallima and Ridi, 2018; Wang *et al.*, 2021). In addition, about five G-Protein Coupled Receptors (GPCRs) are known to be activated by free fatty acid (FFA) ligands (Escribá *et al.*, 2007; Tikhonova, 2016). Lastly, cholesterol in membranes has been found to interact with and modulate a large number of membrane proteins like GPCRs, transporters, and ion channels (Ansell *et al.*, 2021). Moreover, Hedgehog (HH) is an essential molecule required for spatiotemporal control of pattern formation in a developing embryo, which is activated and subsequently exerts its effects in the organism after getting post-translationally modified with a cholesterol molecule (Xu and Tang, 2022).

Taken together, it is evident that along with the widely studied functions of lipids in membrane formation and bioenergetics, these biomolecules are also crucial for performing signalling activities and are capable of modulating diverse physiological pathways. Therefore, it is not surprising that a dysregulation of these lipids is reported in numerous diseases (Wymann and Schneiter, 2008; Wortmann *et al.*, 2014; Nomura and Casida, 2016). However, since these lipid-protein interactions are either not well-categorized and/or the specific protein ligands of a large number of lipids are still unknown, the possible strategies for designing better therapeutic interventions in this area are still at an infancy stage. It is therefore of interest to identify these protein ligands in different cellular systems, both in healthy as well as disease contexts. In this study, we aim to explore the protein interactome of a hitherto unstudied class of lipids-cholesteryl esters.

1.2 Cholesteryl Esters: Known Functions and Possible Fates

Sterols are a class of lipids extensively present across the eukaryotic domain and are known to perform crucial roles in the physiology of a cell. In animal cells, cholesterol and its corresponding esters form the major sterol component (Dufourc, 2008), both known to perform a wide range of functions. Cholesterol is an important constituent of membranes and is essential for maintaining membrane fluidity. In the plasma membrane, it homogenizes the physical properties of membranes to create a new phase called the liquid-ordered phase, which is ideal for supporting biological functions (Marsh, 2010). Moreover, cholesterol is also an important precursor for the biosynthesis of steroid hormones and bile salts (Li and Chiang, 2009). Esterification of cholesterol with fatty acids gives cholesteryl esters (CEs), and this reaction is catalysed by the enzyme Acyl-CoA Cholesterol Acyltransferase (ACAT) in all cells (**Figure 1**). In humans, ACAT is expressed as two isoforms: ACAT1 and ACAT2 (Yu *et al.*, 1996). While ACAT1 is ubiquitously expressed, ACAT2 expression is restricted to the liver and intestine (Reza *et al.*, 2009). In cells, cholesteryl esters are normally present inside the core of lipid droplets along with other storage fats like triacylglycerols (TAGs) (Luo *et al.*, 2019). The formation of cholesteryl esters enables the cells to store excess cholesterol and fatty acids, which in turn helps in the detoxification of cells from excess cholesterol. Moreover, hydrolysis of cholesteryl esters also provides a way to generate free cholesterol when required, a reaction catalysed by cholesteryl ester hydrolases (Zhao *et al.*, 2008; Sakai *et al.*, 2014). The fatty acids in cholesteryl esters produced post hydrolysis can also act as a reserve pool of energy. In addition, cholesteryl esters are a major mode through which sterols are transported to different organs in the body (Fielding and Fielding, 1982). Fatty acids, glycerol, and sterols are transported upon absorption from the gut to the liver in large lipoprotein vesicles called chylomicrons. It has been found that the formation of cholesteryl esters in the intestine by ACAT2 significantly improves cholesterol absorption (Zhang *et al.*, 2012). From the liver, these are transported as Low-Density Lipoprotein (LDL) particles to the peripheral organs, thus delivering dietary cholesterol to the rest of the body. High-Density Lipoproteins (HDL) are responsible for the transport of cholesterol from the peripheral tissues to the liver, a process also known as reverse cholesterol transport, to eliminate excess cholesterol from the peripheral tissues. Hence, HDL is often described as “good” cholesterol, as it helps eliminate

excess cholesterol from the body. Extracellular esterification of cholesterol, which is required to be stored in the core of HDL/LDL particles, is done by the enzyme Lecithin–cholesterol acyltransferase (LCAT) in plasma (Glomset, 1962).

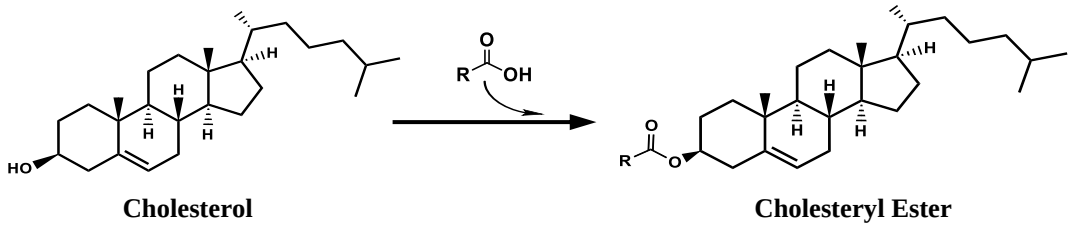

Cholesterol **Cholesteryl Ester**

Figure 1. Biosynthesis of cholesteryl esters from cholesterol. Cholesteryl esters are synthesized by esterification of a fatty acid with the 3' hydroxyl group of cholesterol. This reaction is catalysed by Acyl-CoA Cholesterol Acyltransferase (ACAT) in cells or by Lecithin–cholesterol acyltransferase (LCAT) in plasma.

It is therefore evident that cholesteryl esters have unique roles in the body. However, due to their roles in storage and transport, these molecules were deemed to have inert roles. Over the past few decades, however, there have been several reports highlighting an implication of dysregulation in cholesteryl ester metabolism in numerous diseases. Accumulation of cholesteryl esters in specific regions of the brain (putamen and caudate) has been observed in Huntington's disease (Phillips *et al.*, 2020). Interestingly, since cholesterol is majorly synthesized de novo in the brain as dietary cholesterol cannot readily cross the blood-brain barrier, increased levels of cholesteryl esters in these regions may reflect their specific intrinsic activity in this disease-specific context. Moreover, such elevated levels of these esters are also reported in Amyotrophic Lateral Sclerosis (ALS), where along with ceramides they induce oxidative stress, leading to the death of motor neurons (Cutler *et al.*, 2002). However, the consequences and exact mechanistic understanding of increased levels of cholesteryl esters remain unknown in both Huntington's and ALS. Additionally, whether individual esters with differing lengths of fatty acyl chains possess differential activity remains to be studied. Apart from this, cholesteryl esters are now increasingly becoming known to affect the pathogenesis of Alzheimer's disease (Proitsi *et al.*, 2015; Van Der Kant *et al.*, 2019; Chang *et al.*, 2021). It is known that these esters regulate the accumulation of phosphorylated Tau (pTau) and amyloid-beta (Aβ) fragments,

both of which are regarded as major hallmarks of Alzheimer's disease. Evidence suggests that cholesteryl esters regulate the accumulation of these two proteins via independent pathways. Intriguingly, pTau accumulation was found to be mediated by inhibition of the proteasomal machinery by cholesteryl esters, and both inhibition of ACAT and reduction in existing cholesteryl esters reduced pTau levels (Van Der Kant *et al.*, 2019). While it was found that the effect of cholesteryl esters on proteasomal subunits was not regulated at the transcriptional level, it remains to be found whether this inhibition occurs by direct binding of cholesteryl esters to proteasomal subunits in a concentration-dependent manner, or whether these esters bind to a yet another protein which binds to and thereby inhibits the proteasome. Further, cholesteryl ester accumulation in macrophages is a classic characteristic of the formation of foam cells, which are central to the pathoprogression of atherosclerotic plaques. Oxidized cholesteryl esters (Ox-CEs), formed during atherosclerosis are also increasingly being recognised as pro-inflammatory moieties, which further fuel pro-atherogenic activities (Leitinger, 2003; Choi *et al.*, 2017). Lastly, an aberrant increase in cholesteryl ester levels has also been reported in cancers, where an inhibition in cholesterol esterification was shown to hamper cancer aggressiveness (Yue *et al.*, 2014; Li *et al.*, 2016; Liu *et al.*, 2022).

All in all, cholesteryl ester dysregulation has been implicated in various neurological, inflammatory, and neoplastic diseases, but whether these molecules play a role in influencing protein activities upon interaction remains unknown. While there have been extensive studies on understanding protein-cholesterol interactome (Hulce *et al.*, 2013), protein-cholesteryl ester interactions still remain a topic of much experimentation and discussion. Due to this, the identification of the specific protein ligands for these molecules on a proteome-wide scale is important. Taken together, we hypothesize that cholesteryl esters may perform crucial roles in signalling, apart from their reported roles in storage and transport. This function could be important in normal homeostasis and might be disrupted during disease, knowledge of which would be imperative for the identification of novel therapeutic targets.

1.3 Strategy: Photoreactive Bioorthogonal Lipid Probes

Traditional methodologies identifying lipid-protein interactions relied mostly on conventional biochemical techniques such as affinity chromatography, surface plasmon resonance (SPR), isothermal calorimetry, thermal shift assays, or computational methods like in-silico modelling and docking studies. While these techniques provided a solid foundation for studying these interactions, they were primarily limited to in vitro systems and lacked a proteome-wide coverage. With the latest advancements in bioorthogonal chemical reactions and state-of-the-art mass spectrometry-based chemoproteomics, it has become possible to map lipid-protein interactions at a proteome-wide scale using multifunctional lipid probes, thus enabling the identification of previously unknown protein ligands inside various mammalian cells and tissues. Over the past decade, such type of lipid probes were developed and utilised, expanding our knowledge of their applications in various cellular systems. The first class of photoreactive probes were synthesized for phosphatidylcholines (PCs) (Gubbens and De Kroon, 2010; Xia and Peng, 2013), and then other groups expanded their usage to phosphatidylinositol-tri-phosphates (Rowland *et al.*, 2011), cholesterol (Hulce *et al.*, 2013), and arachidonoyl lipids (Niphakis *et al.*, 2015). These studies could identify the interacting proteins at a proteome-wide scale, could confirm the already known interactors, and more importantly, numerous novel interactors were also found for these lipids. In our study, we make use of photoreactive bioorthogonal lipid probes to explore the interactome of a hitherto unstudied class of lipids-cholesteryl esters.

The basic design of the probe involves an additional photoreactive group and a bioorthogonal handle appended to the parent lipid (**Figure 2A**). Upon activation by a particular wavelength of light, the photoreactive group forms a reactive intermediate which crosslinks to the interacting protein in the vicinity. This enables the formation of stable, covalently bound, lipid-protein complex and is hence capable of capturing the usually non-covalent, weak, and/or transient lipid-protein interactions. On the other hand, the bioorthogonal moiety in the probe can be used to tag the protein-probe complex with a fluorescent or an affinity handle using what is known as the “click reaction” (**Figure 2D**), allowing the downstream analysis of the protein-probe complex to be amenable (**Figure 2C**). For example, a fluorescent tag can be used to perform

an in-gel fluorescence analysis, or can be used to visualize this complex inside cells using fluorescence microscopy. If attached with an affinity handle, the complex can be isolated using pulldown experiments and the attached protein can be identified using mass spectrometry-based proteomics. In addition, since the bioorthogonal tag is a terminal alkyne or azide, this type of lipid probe mimics the parent lipid much more closely than conventionally used bulky fluorescent/affinity attachments. This property is imperative for screening and identification of specific interactors of the natural lipid. The photoreactive moiety used in the lipid probes of our study is a diazirine ring. This diazirine moiety is activated with UV exposure (330 nm to 370 nm), forming a highly reactive carbene intermediate, which can then undergo an addition reaction onto the peptide backbone of the interacting protein, forming a stable covalent adduct (West *et al.*, 2021). Moreover, since the diazirine group is a relatively small moiety, it adds to the value of being able to resemble the natural lipid. The bioorthogonal handle used in the probes is a terminal alkyne, which is amenable to click chemistry. Amongst the available types of click reactions, we use Copper assisted Azide-Alkyne Cycloaddition (CuAAC) type of click reaction (Haldón *et al.*, 2015). In this reaction, Cu(I) catalyses the 1,3-dipolar cycloaddition between the terminal alkyne of the probe and azide group of reporter tag, hence enabling attachment of the reporter tag to the probe. At this point, it is also worth mentioning that Carolyn Bertozzi, K. Barry Sharpless and Morten Meldal were jointly awarded the 2022 Nobel Prize in Chemistry, for their contributions in bioorthogonal chemistry, considering its applicability in a plethora of biological systems.

Design of the cholesteryl ester probe: Since animal cells usually have an even number of carbons in fatty acids, with 16-20 carbon units being most abundant, we decided to have a palmitate (16-C saturated fatty acid) moiety esterified to the cholesterol head group, to mimic the natural substrate. The diazirine moiety is attached to the C-11 position of the fatty acid. A terminal alkyne is present as the bioorthogonal handle. The probe is named Cholesteryl Palmitate Diazirine Alkyne (hereafter referred to as CPDA) (**Figure 2B**).

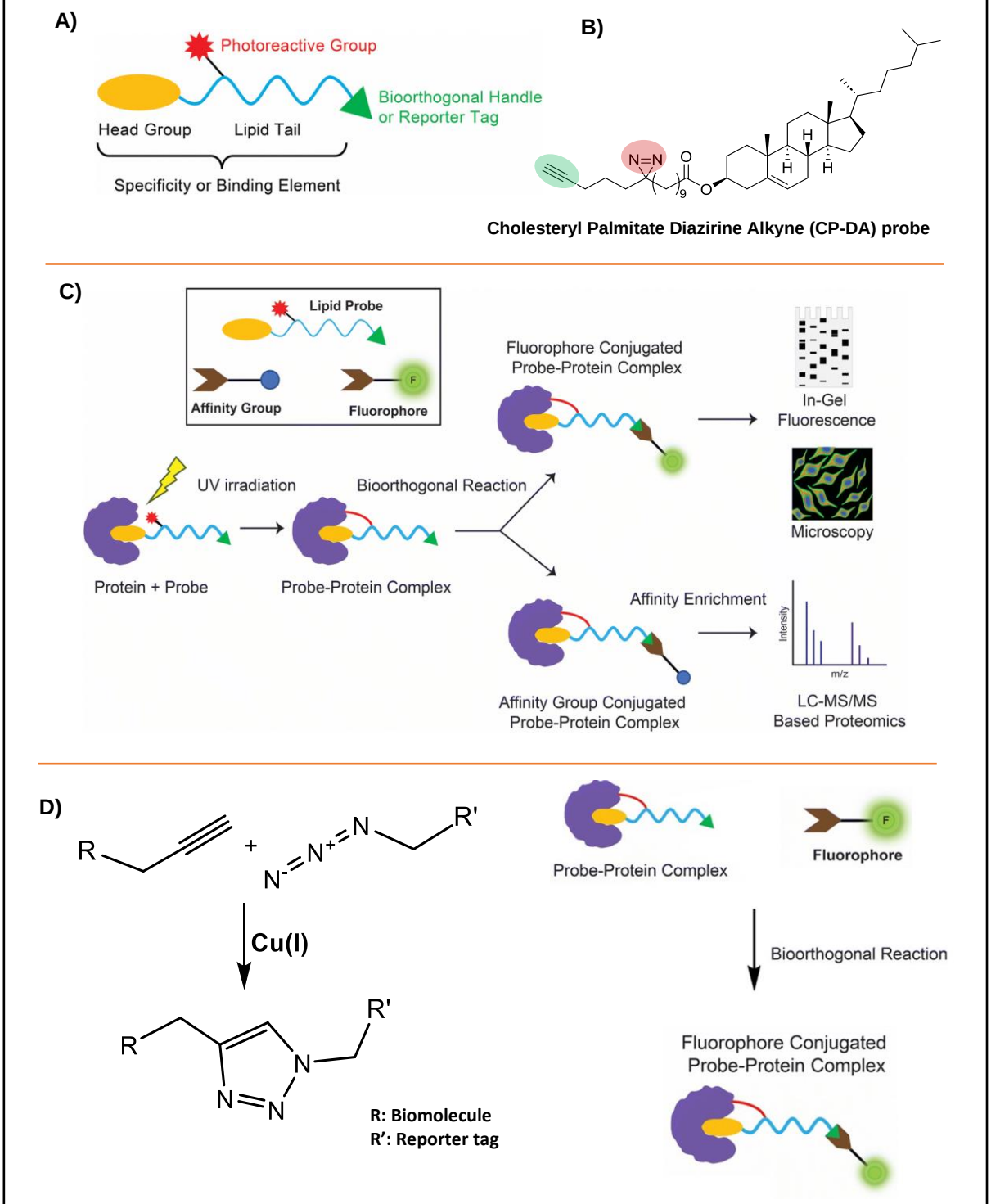

Figure 2. Strategy for utilisation of bioorthogonal lipid probes. A) Generic structure of lipid probes. Along with the natural lipid, which acts as the specificity element which the interacting proteins recognise, two additional groups are present: photoreactive group and bioorthogonal handle (Shanbhag et al., 2023) B) Structure of CPDA probe used in the study C) Schematic for usage of probe: photoreactive group helps in formation of a stable, covalently bound protein-probe adduct upon UV irradiation, and biorthogonal handle can be used to analyse this adduct via in-gel fluorescence, microscopy or proteomics (Shanbhag et al., 2023). D) Schematic of Copper catalysed Azide-Alkyne cycloaddition (CuAAC) reaction, a type of bioorthogonal chemical reaction used in the study, to append a fluorophore or affinity group onto the probe.

Bioorthogonal probes for chemoproteomic competition: The cholesteryl ester probe can also pull-down proteins interacting only with the sterol ring or the iso-octyl tail and not the ester moiety as a whole. To screen for proteins specific to cholesteryl esters and not only to cholesterol/sterol ring region, we use a bioorthogonal cholesterol probe to compete with the ester probe in a chemoproteomic competition. The cholesterol probe has a diazirine ring in attached onto the sterol ring and the alkyne handle is etherified to the oxygen using a propargyl group. This probe would effectively eliminate protein targets specific to the sterol region. The cholesterol probe is named Cholesterol Diazirine Alkyne (hereafter referred to as ChDA) (**Figure 3A**). Similarly, the ester probe can also pull-down proteins that recognise only the fatty acyl chain. To eliminate such proteins a free fatty acid probe should be competed with the ester probe. Therefore, a palmitic acid probe (free fatty acid probe), which is the same fatty acid esterified in the ester probe, is used for this purpose. The fatty acid probe is named Palmitate Diazirine Alkyne (hereafter referred to as PADA) (**Figure 3B**).

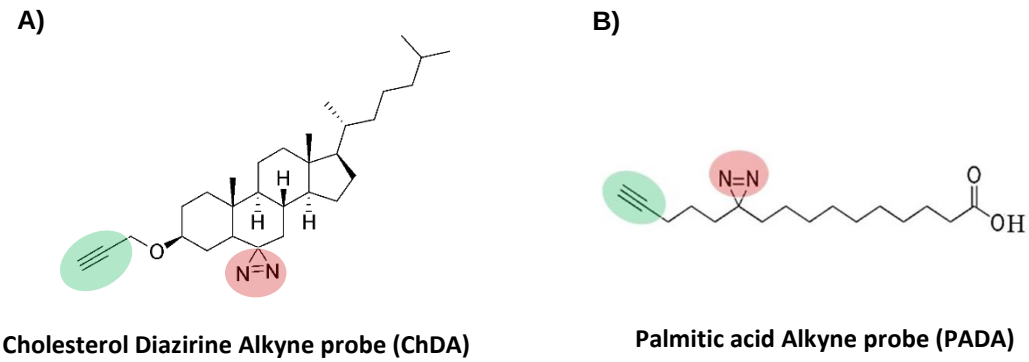

Figure 3. Biorthogonal probes for competition. A) Structure of cholesterol probe (ChDA) used to compete with the ester probe for the sterol region B) Structure of free fatty acid probe (PADA) used to compete with the ester probe on the fatty acyl region

Chapter 2 Materials and Methods

2.1 Materials and Reagents

Media

Reagent	Source	Identifier
Dulbecco's Modified Eagle Medium (DMEM)	HIMEDIA	AL066A
Roswell Park Memorial Institute (RPMI)	HIMEDIA	AL028A
Foetal Bovine Serum (FBS)	HIMEDIA	RM1112
Penicillin-Streptomycin (PS)	MP Biomedicals	1670249

Vehicles for probe delivery

Reagent	Source	Identifier
Dimethyl sulfoxide (DMSO) (HPLC grade)	Merck	5.43900.1000
Methyl beta-cyclodextrin (MβCD)	Sigma	C4555

Protein Estimation

Reagent	Source	Identifier
Bovine Serum Albumin	Sigma	A2153
Bradford's Reagent	Sigma	B6916

Click Chemistry

Reagent	Source	Identifier
TBTA	Sigma	678937
$CuSO_4.5H_2O$	Merck	MD6M561035
TCEP	Sigma	C4706
Rhodamine-Azide	Sigma	760765
Biotin-Azide	Sigma	762024

Polyacrylamide Gel Electrophoresis

Reagent	Source	Identifier
Tris-base	HIMEDIA	TC072
SDS	HIMEDIA	MB010
Acrylamide	HIMEDIA	MB068
Bis-acrylamide	HIMEDIA	MB005
Ammonium persulfate	Sigma	A3678
TEMED	Sigma	T9281
Glycine	Qualigens	Q24755
Propan-2-ol	Qualigens	Q13825

Proteomics

Reagent	Source	Identifier
Methanol (MS Grade)	JT Baker	BAKR9830-03
Chloroform (MS Grade)	Sigma	650498

Urea	Sigma	U5128
K_2CO_3	Sigma	243558
Iodoacetamide	Sigma	I1149
Trypsin	Promega	V5111
Avidin-Agarose Beads	Sigma	A9207
Triethylammonium Bicarbonate buffer	Sigma	90360
Formaldehyde (CH_2O)	Sigma	252549
Heavy Formaldehyde (CD_2O)	Cambridge Isotope Laboratories, Inc.	DLM-805-20
Sodium Cyanoborohydride	Sigma	156159
28% Ammonium Hydroxide	Sigma	338818
Trifluoroacetic acid	Sigma	302031
C-18 disc	Supelco	66883-U

2.2 Cell Culture

Culturing of secondary cell lines

Four secondary cell lines were considered for this study: RAW 264.7 (murine macrophages), Neuro 2a (N2a, murine neural crest cells), BV2 (murine microglial cells), and HEK293T (Human Embryonic Kidney cells). All the cells were cultured in polystyrene adherent plates at 37°C and 5% CO_2 levels. All the cells, except HEK, were cultured in Dulbecco's Modified Eagle Medium (DMEM), while HEK cells were cultured in Roswell Park Memorial Institute (RPMI) medium with 5% penicillin-streptomycin (PS). Since RAW 264.7 and BV2 are known to get activated by the

complement system, heat-activated (at 60°C for 1 hr) 10 % foetal bovine serum (FBS) was used for these cells while native 10% FBS was used for N2a and HEK cell lines.

Culturing of primary murine macrophages

All mouse studies received formal approval from the Indian Institute of Science Education and Research, Pune Institutional Animal Ethics Committee (IISER-P IAEC), in accordance with the official norms provided by the Committee for the Purpose of Control and Supervision of Experiments in Animals (CPCSEA), Government of India. Eight- to ten-week-old C57BL/6J mice (obtained from Jackson Laboratory) were induced sterile inflammation by injecting thioglycolate intra-peritoneally to trigger differentiation of monocytes to peritoneal macrophages. After three days, these mice were anaesthetized using CO_2 and were then euthanised via cervical dislocation. 10 mL Dulbecco's Phosphate Buffered Saline (DPBS) (4°C) was then injected into the peritoneal cavity of these mice, careful enough not to puncture any organ. The abdominal cavity was gently tapped to suspend the macrophages inside the body in the injected DPBS. Then, the DPBS was recollected and stored in a falcon. Post collection, the fluid was centrifuged at 4°C at 1500 RPM for 5 min. The supernatant was aspirated and the residual cell pellete was resuspended in 5 ml RBC (Red Blood Cell) Lysis buffer (155mM NH_4Cl + 12mM $NaHCO_3$ + 0.1mM EDTA) with gentle pipetting. This was incubated for 15 min at 4°C and then centrifuged again at 4°C at 1500 RPM for 5 min. The supernatant was aspirated and the cell pellete was resuspended in RPMI media. The cells were plated in adherent polystyrene cell culture plates as per desired seeding density. Fresh media was added after four hours to remove dead cells and debris.

2.3 Probe delivery methods

Both the sterol probes were delivered in cells using two methods:

1. **In DMSO solvent:** Since both the probes were sparingly soluble in DMSO when directly added, they needed to be solubilised using sonication. First, a 10mM stock solution of the probe was prepared, and then it was sonicated in a water-bath sonicator for 30 min at 45°C. It was then probe-sonicated at 50% amplitude for five pulses. This probe solution was directly stored at -40°C until used for incubating the cells.

2. **Using methyl-beta-cyclodextrin (MβCD) in PBS**: The usage of MβCD for delivering cholesterol to the cells is well-established (Christian et al., 1997), however, delivering cholesteryl esters using this method was tested for the first time for this study. The probe and MβCD were added to PBS in a 1:10 ratio (probe: MβCD), and a stock solution of 1mM was prepared. This mixture was kept in a water-bath sonicator and was put for one degassing cycle followed by 15 min water-bath sonication at 30-35°C. The solution was then immediately kept for incubation at 37°C for 14 hr with gentle mixing (180 RPM). The solution was then filter sterilized using a 0.45µm syringe filter and was then stored at room temperature until further use.

Protein estimation

Since the use of equal protein concentration in both control and test samples is necessary, protein present in the cell lysates was estimated using Bradford's assay. Protein from the samples was diluted to Bradford reagent's range (0.5- 1.2mg/mL). Standard Bovine Serum Albumin (BSA) stock solutions from 0 to 1mg/mL were used to generate a standard curve for comparison. Around 200µL of Bradford's reagent (which contains Coomassie G-250 dye) was added to 10µL of diluted sample and BSA stock solutions. The absorbance was measured at 595nm. Using Beer-Lambert's law, the unknown protein concentration was estimated using the linear equation obtained from the standard curve. The samples, before setting up the click reaction, were hence made to desired protein concentration; for example, 1mg/mL of protein concentration was used for proteomics experiments.

2.4 Click chemistry

The reagents used for the click reaction are 1.5mM tris-(benzyltriazolylmethyl)amine (TBTA), 50mM Copper Sulfate ($CuSO_4$), 50mM tris(2-carboxyethyl) phosphine (TCEP), and Rhodamine azide (10 mM in DMSO) [or biotin-azide for proteomics] in 6:2:2:1 ratio, respectively (total 11µL click reagent mixture for 100µL lysate). The reaction was carried out on a thermomixer at 25°C for 1 hr at 800 RPM.

2.5 In-gel fluorescence analysis

SDS-PAGE (Sodium Dodecyl Sulfate- Polyacrylamide Gel Electrophoresis) was used to separate the protein-probe complexes. The gels were run at 10% resolving and 4% stacking. Rhodamine azide handle is used to detect the proteins interacting with the

probe. The gels were imaged in an iBright 4000 gel imager under protein fluorescence settings.

2.6 Microscopy

Cells were allowed to adhere onto coverslips, placed inside cell culture plates. The probe was incubated at 50μM concentration and then cells were UV irradiated post incubation period. The cells were then fixed with ice-cold methanol for 15 min. Cells were then washed with isopropanol followed by chloroform/methanol/acetic acid (10/55/0.75 v/v) for 2 min each. These washes ensure any probe unbound to protein is washed off. Cells were then washed with PBS and subjected to CLICK reaction mixture to attach rhodamine tag onto the probe for visualization. The reagents used to prepare the CLICK reaction mixture were TBTA (100μM), $CuSO_4$ (1mM), TCEP (1mM), and Rhodamine-azide (2μM). This was followed by PBS wash and the cells were then incubated with 4',6-diamidino-2-phenylindole (DAPI) for 5 min and then mounted in antifade. Imaging was done using a 63x objective on a Zeiss LSM770 confocal microscope, and image analysis was done using Fiji software.

2.7 Lipidomics

Both the samples, test (i.e., probe-treated cells) and control (i.e., vehicle-treated cells), were harvested and resuspended in 1 mL DPBS. Appropriate internal standards were mixed in chloroform, and 2 mL of this mixture was added to each sample. For the cholesteryl ester probe, cholesterol esterified to a 17-carbon fatty acid was used as an internal standard, and a concentration of 1 nmol/μL was added to each sample. For the cholesterol probe, deuterated cholesterol (d7) was used at 2 nmol/μL as an internal standard. 1mL of methanol was added to the samples and vortexed. It was then centrifuged at 3000 RPM for 15 min. The neutral lipids are enriched in the lower organic layer thus formed post centrifugation. Hence, around 1500 μL of the organic layer was collected and transferred to a new glass vial. 50 μL formic acid was then added to the remaining solution and vortexed. An additional 2 mL of chloroform was added in the vial and vortexed. This step ensures that the anionic lipids that remain in the aqueous layer can then be enriched in the organic layer post centrifugation. 2 mL of this newly formed organic layer was carefully collected and added to the previously collected 1.5 mL organic solution. The final 3.5 mL organic layer was dried in a stream of inert N_2 gas. After drying, 1 mL of chloroform was added to the vial and transferred

to a new glass vial, leaving the residual aqueous contamination that may be present. This was again dried in a stream of N_2 gas and stored at -80°C. For mass spectrometry analysis, 200 µL of 2:1 $CHCl_3$: MeOH mixture was added to the vial and half of it was sent for mass spectrometry runs. The samples were processed in an LC-ESI-QTOF machine and were analysed using the Agilent LC-MS software.

2.8 Proteomics

Post probe incubation and UV irradiation as mentioned before, cell lysate was subjected to CLICK reaction and biotin-azide was covalently attached to the probe-protein complex. This biotin-labelled lysate was mixed with 2 mL MeOH, 0.5 mL $CHCl_3$ and 1 mL PBS, vortexed, and centrifuged at 3500g for 15 min to separate the protein disc. The protein disc forms at the interface of the organic (bottom) and the aqueous (top) layers. The organic and aqueous layers were aspirated and the intact protein disc was washed thrice with 1:1 MeOH: $CHCl_3$ mixture. The protein disc was then denatured, reduced, and solubilised using 6M Urea (in PBS), 10% SDS and 1:1 TCEP (200mM): K_2CO_3 (600mM) mixture, in a water-bath sonicator. The solution was then subjected to Iodoacetamide (55µM) to alkylate the thiol group of cysteine residues, preventing it from forming disulfide bonds in future steps. This mixture was then incubated with avidin beads for 2.5 hours to allow the biotin-labelled probe-protein complex to be bound onto the beads. Post incubation, the beads were washed thrice with 0.2% SDS (at 250g),1X PBS (at 500g) and Milli-Q (at 800g) to remove non-specific proteins and enrich the proteins bound with the probe. The beads were then subjected to trypsin digestion in 2M urea/100mM TEAB (triethylammonium bicarbonate) buffer. Post trypsin digestion, the generated peptides were subjected to Reductive Dimethylation Labelling (ReDiMe). When peptides are treated with formaldehyde and sodium cyanoborohydride, the N-terminal and lysine side-chain primary amines undergo dimethylation reaction (**Figure 5**). The control samples (-UV) were labelled with 8% light formaldehyde (CH_2O) whereas the test samples were labelled with 8% heavy formaldehyde (CD_2O) enabling differential labelling in both the samples. The ReDiMe reaction was quenched with 8% ammonium hydroxide solution after 1 hour. 20% trifluoroacetic acid (TFA) was added to the samples. The labelled control and test samples were then mixed and proceeded for desalting. Desalting was done using zip-tips packed with C-18 discs. The C-18 disc was activated using 50µL 100% acetonitrile (ACN), and was then equilibrated using 60µL 0.1% tri-fluoroacetic

acid (TFA). The peptides were then loaded onto the disc, which was followed by 120µL 0.1% TFA to remove salts. The peptides were then eluted in 60µL 60% ACN (in 0.1% TFA) and dried at 40°C in a vacuum concentrator. The peptides were then sent for LC-MS/MS analysis. Peptides were run in a nano-LC-ESI-QTOF mass spectrometer, and the resulting spectra were analysed using ProteinPilot software. **Figure 4** shows the schematic for the proteomics done in the study.

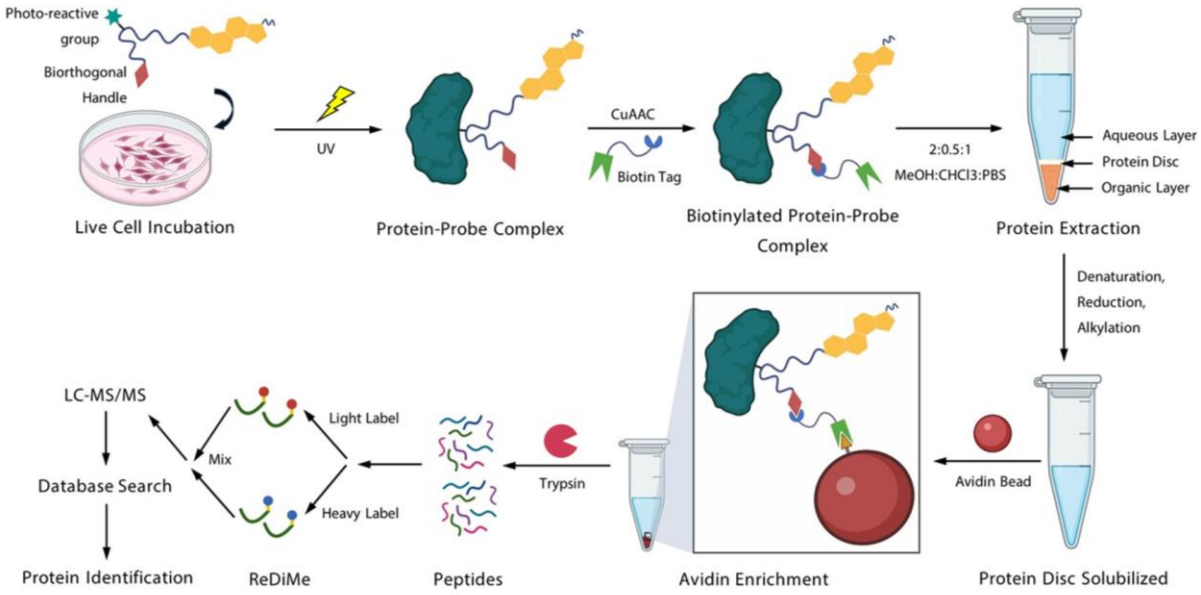

Figure 4. Schematic for proteomics workflow. Post incubation and UV crosslinking, the probe-protein complex can be tagged with an affinity group like biotin-azide and the interacting proteins are enriched using avidin beads. The enriched proteins can then be digested using trypsin enzyme to generate peptides. The peptides from the test and the control samples can be labelled differentially using Reductive Dimethylation Labelling (ReDiMe), and then mixed later to be run together in the liquid chromatography coupled mass spectrometer (LC-MS/MS). The generated spectra from LC-MS/MS can be analysed using existing peptide libraries to finally identify the interacting protein.

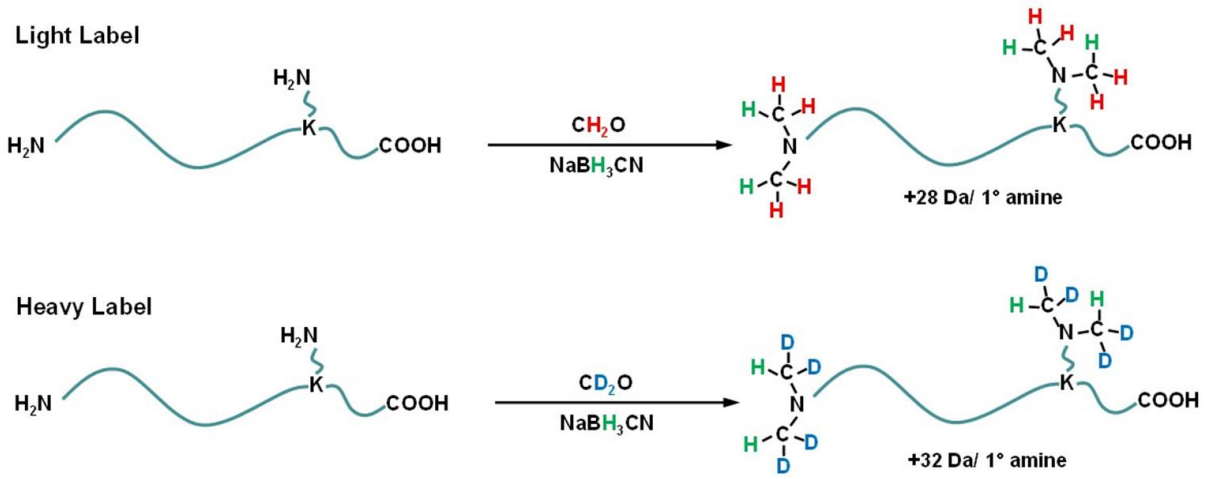

Figure 5. Reductive Dimethyl Labelling (ReDiMe). ReDiMe can be used to differentially label and hence identify peptides generated from control vs. test samples. By using heavy formaldehyde (CD_2O), a mass difference of +4 can be obtained in heavy labelled samples as compared to the light labelled ones. Since isotopes have similar chemical properties, these peptides co-elute, and the ratio of peak intensities directly gives the proteins obtained from respective samples.

Chapter 3 Results

3.1 Standardizing conditions for optimal probe uptake

3.1.1 Optimizing CPDA probe usage in cell lines

The first aim of our study was to assess the applicability of the chemically synthesized probe in possibly relevant biological systems. A stock solution of 10mM of the probe was made in DMSO initially, and it was tested to see if the probe interacts with cellular proteins using cell lysates. As mentioned before, the resulting lipid-protein interaction was analysed using in-gel fluorescence analysis, by clicking the probe with rhodamine-azide. However, even at probe concentrations as high as 1mM, a significant intensity of protein bands was not seen on the polyacrylamide gel. The probe was then tested in a live-cell incubation experiment, but even then, a significant protein band intensity on the gel was not observed. Following up, since the CPDA probe is highly lipophilic, we tried to enhance the probe solubility in DMSO using sonication (more details in Materials and Methods). Along with this, the probe was also incubated in live cells in serum-free media to prevent the binding of the probe to FBS proteins in the cell culture media. This was initially assessed in multiple cell lines at varying concentrations (maximum till 50μM) for 30 min incubation time. The UV exposure treatment was done for 10 min to cross-link the interacting proteins. The controls used in the experiment were vehicle control (i.e., DMSO/ no probe control) and no UV control (i.e., no UV irradiation, but in the presence of probe). This time, although at less intensity, we could see protein bands in the RAW 264.7 cell line; however, no bands were still seen in other cell lines like N2a and HEK 293T (**Figure 6 A-C**). Since the maximum amount of probe that can be incubated in cell lines is limited by excess probe/DMSO-associated toxicity, we decided to increase the incubation time of the probe at 50μM. From 30 min to 4hr incubation time, we could see a steady increase in the intensity of protein bands in RAW 264.7 cell line (**Figure 6 D**). Moreover, an important observation to be considered is that nearly all of the interactions were UV-dependent, suggesting that almost all of these interactions are non-covalent in nature. As for the other cell lines, N2a showed protein bands only at 4hr incubation and not before, suggesting that probe uptake by these cells is not at a steady rate, and is likely not taken up

immediately after probe addition (**Figure 6 E**). For BV2, the intensities were nearly similar at 2hr and 4hr time scales, indicating a possible saturation of probe uptake after 4hr (**Figure 6 G**). Interestingly, HEK 293T showed only one protein band at an appreciable intensity (**Figure 6 F**). Taking these observations into consideration, 50µM probe concentration at 4hr incubation time was considered optimal for cellular uptake. These incubation conditions were also tested for primary macrophages, and a considerable number of interacting proteins could be observed (**Figure 6 H**). Hence, we decided to proceed further with RAW 264.7, N2a, BV2, and primary macrophage cells for further analyses. In addition, since the probe-protein interaction was now qualitatively established using the in-gel fluorescence analysis, we sought to repeat using the better dissolved probe in cell lysates. However, the probe still failed to interact with proteins in the lysate (data not shown). Therefore, we decided to proceed with live-cell treatment, and went ahead to test the ChDA probe in these cell lines.

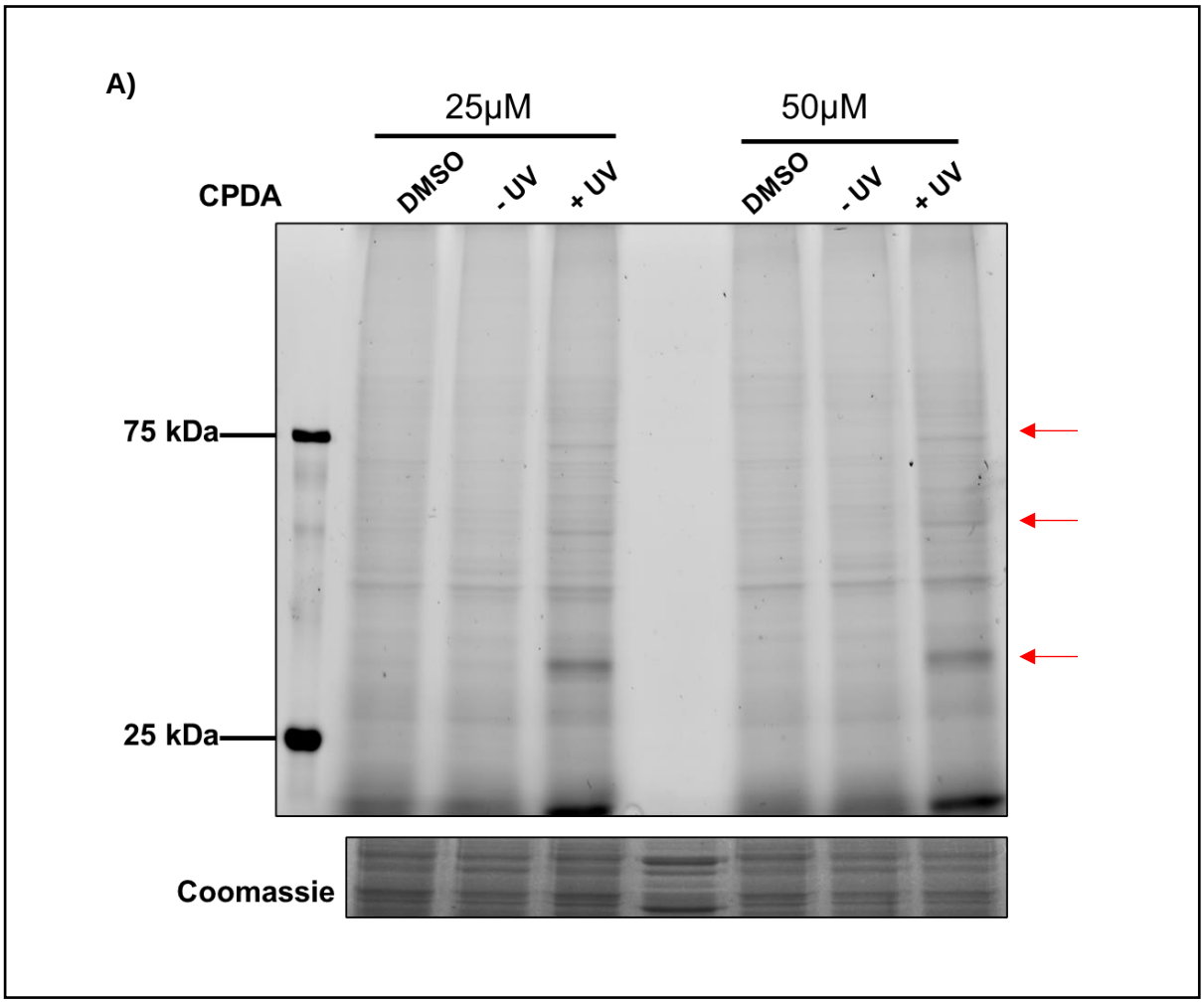

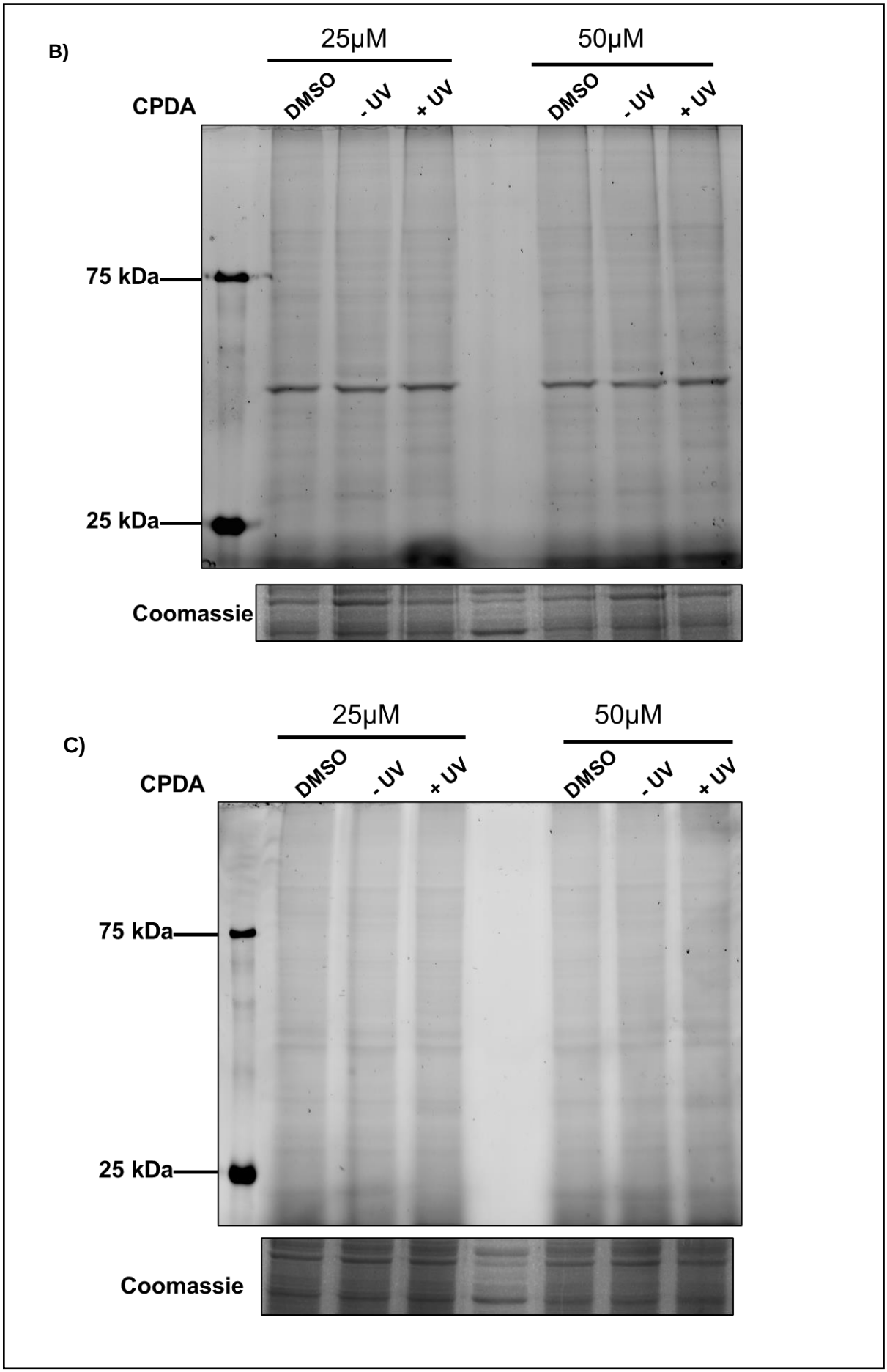
B)
25μM
50μM
CPDA
DMSO
- UV
+ UV
DMSO
- UV
+ UV
75 kDa
25 kDa
Coomassie
C)
25μM
50μM
CPDA
DMSO
- UV
+ UV
DMSO
- UV
+ UV
75 kDa
25 kDa
Coomassie

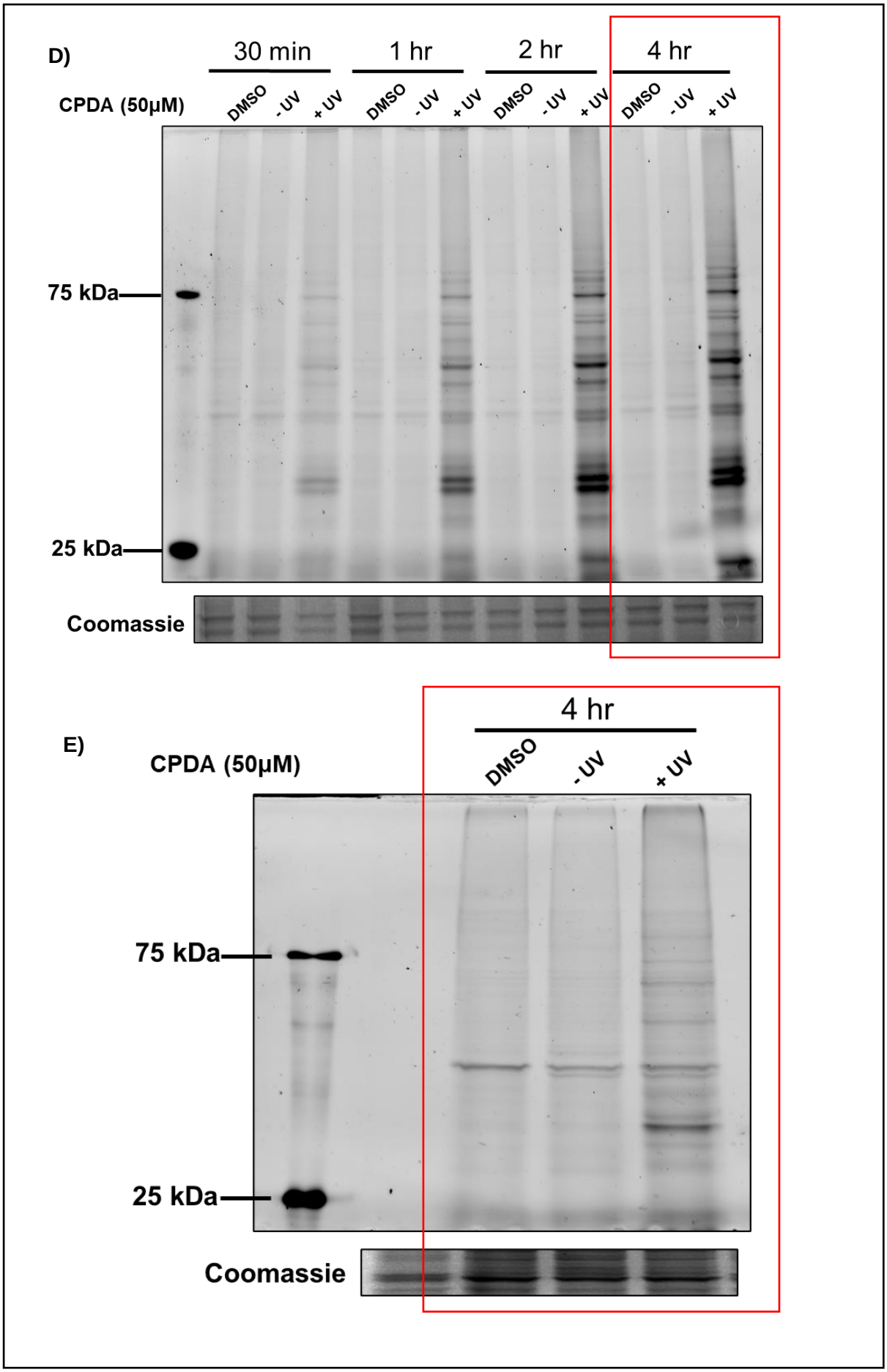
D)
30 min
1 hr
2 hr
4 hr
CPDA (50μM)
DMSO
- UV
+ UV
75 kDa
25 kDa
Coomassie
E)
4 hr
CPDA (50μM)
DMSO
- UV
+ UV
75 kDa
25 kDa
Coomassie

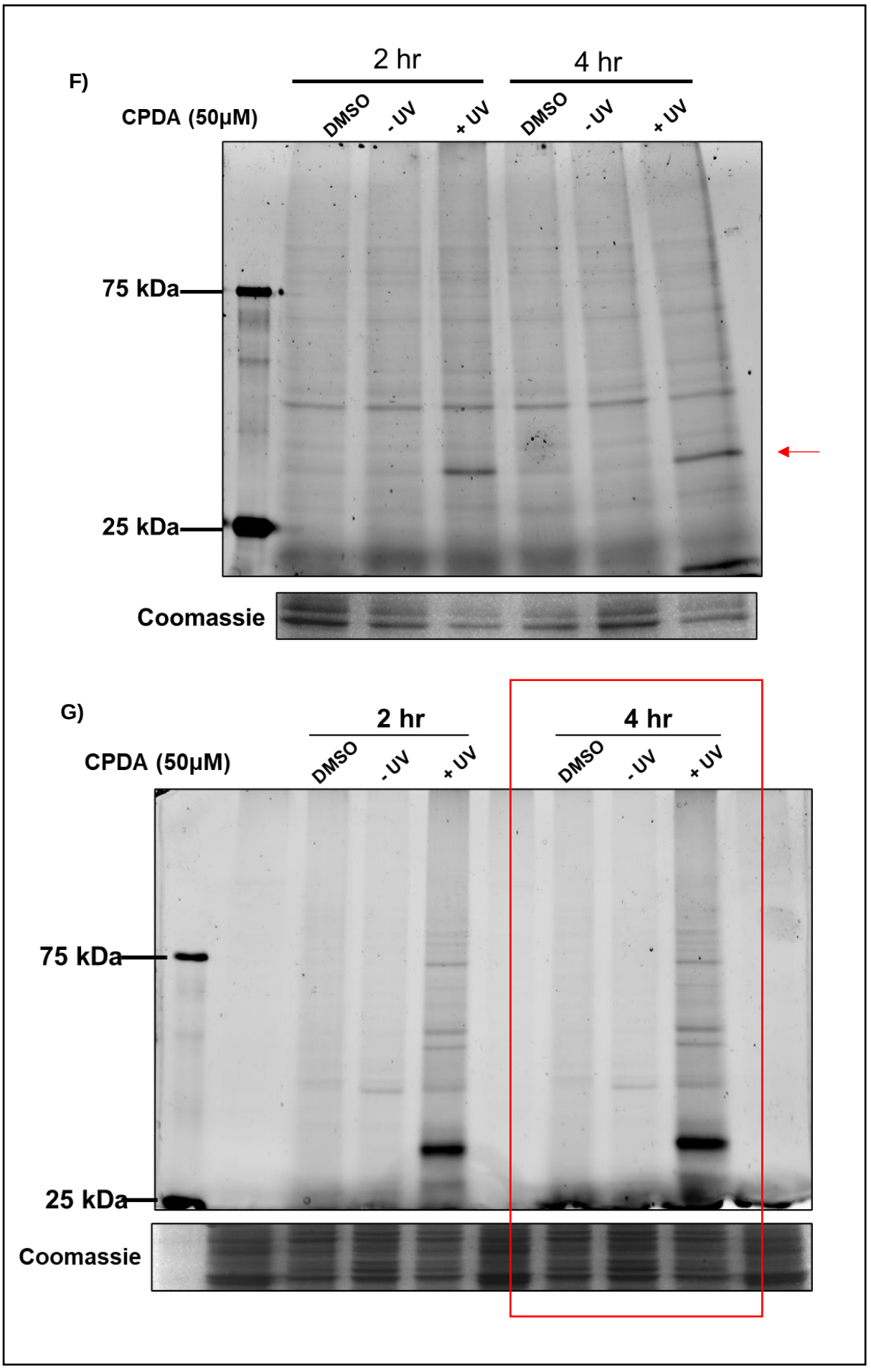
F)
2 hr
4 hr
CPDA (50μM)
DMSO
- UV
+ UV
DMSO
- UV
+ UV
75 kDa
25 kDa
Coomassie
G)
2 hr
4 hr
CPDA (50μM)
DMSO
- UV
+ UV
DMSO
- UV
+ UV
75 kDa
25 kDa
Coomassie

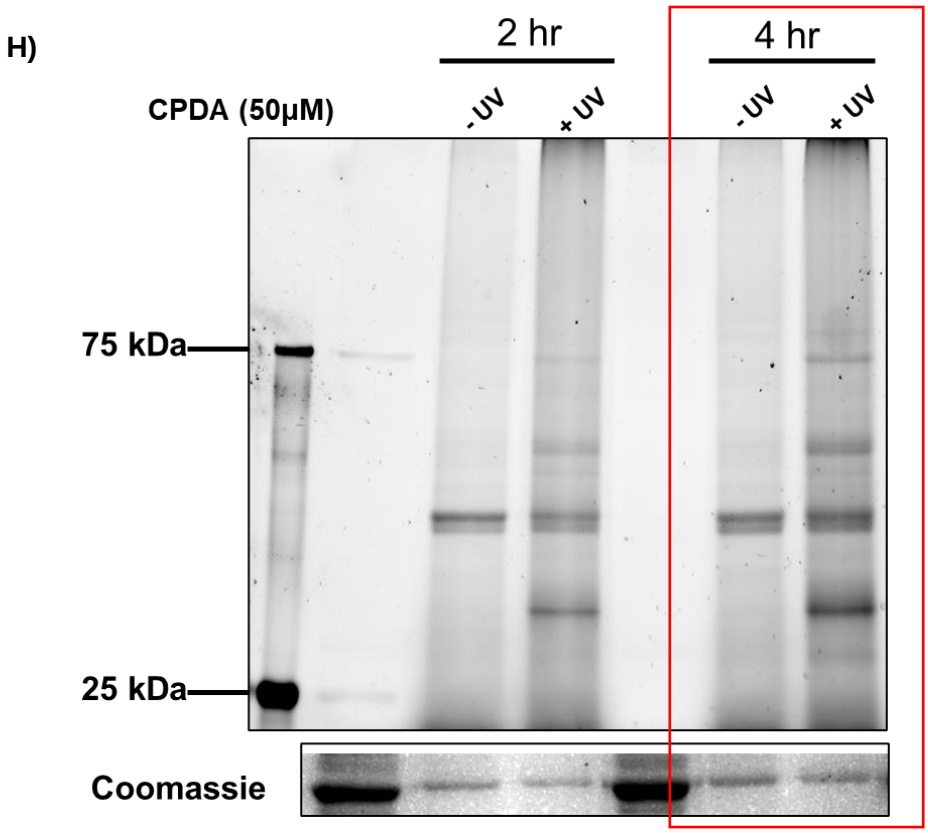

Figure 6. Optimising CPDA probe usage in cell lines. A-C) In-gel fluorescence for 25-50μM concentration at 30 min incubation in RAW 264.7, N2a, and HEK 293T, respectively. D-H) In-gel fluorescence for 50μM concentration at varying incubation times in RAW 264.7, N2a, HEK 293T, BV2, and primary macrophages, respectively.

3.1.2 Optimizing ChDA probe usage in cell lines

After optimizing the CPDA probe, the cholesterol probe (ChDA) to be used for chemoproteomic competition was tested in the shortlisted cell lines at 50μM concentration. The UV exposure time was continued to be kept at 10 min. In RAW 264.7, surprisingly, the protein bands were most significant at 4hr incubation, and compared to CPDA, a steady increase was not observed. Instead, marginal protein band intensity was observed at 2 hours, and no protein bands were seen at 1 hour of incubation (**Figure 7 A**). When incubated in N2a, a similar trend as CPDA was observed wherein only 4hr incubation resulted in appreciable protein-probe interaction (**Figure 7 B**). However, in BV2, a similar trend as CPDA was captured, wherein 2-hour and 4-hour incubations were not significantly different (**Figure 7 C**). In line with these

observations, we sought to test the probe in primary macrophages, and we could observe significant protein interactors at 4-hour incubation time and 50µM concentration with the ChDA probe as well (**Figure 7 D**). To note, the ChDA probe also failed to interact with proteins in cell lysates (data not shown). This observation may possibly indicate that the proteins interacting with both the probes may require the in-situ microenvironment for optimal activity. However, this could also mean that the probes are still possibly precipitating out when they come in contact with the aqueous cellular environment. Nevertheless, it was established that both the probes could be used at 50µM and 4hr incubation in live-cell treatments. To further compare the probes, we ran the samples (in RAW264.7, BV2) treated with either of the probes together in the same gel. Interestingly, we could observe that the ChDA probe interacted with far more proteins and at a higher band intensity (**Figure 7 E, C**). It should also be noted that we observe fewer bands in the CPDA lane than before since higher intensity of ChDA bands mask the lower intensity bands of the CPDA probe, taken at a lower fluorescence exposure time in the gel-imager instrument. Lastly, the PADA probe, which is also to be used for competition experiments, was optimized before in previous studies, and it bound to proteins in both live cells and lysates at 50µM at 30 min incubation time (data not shown).

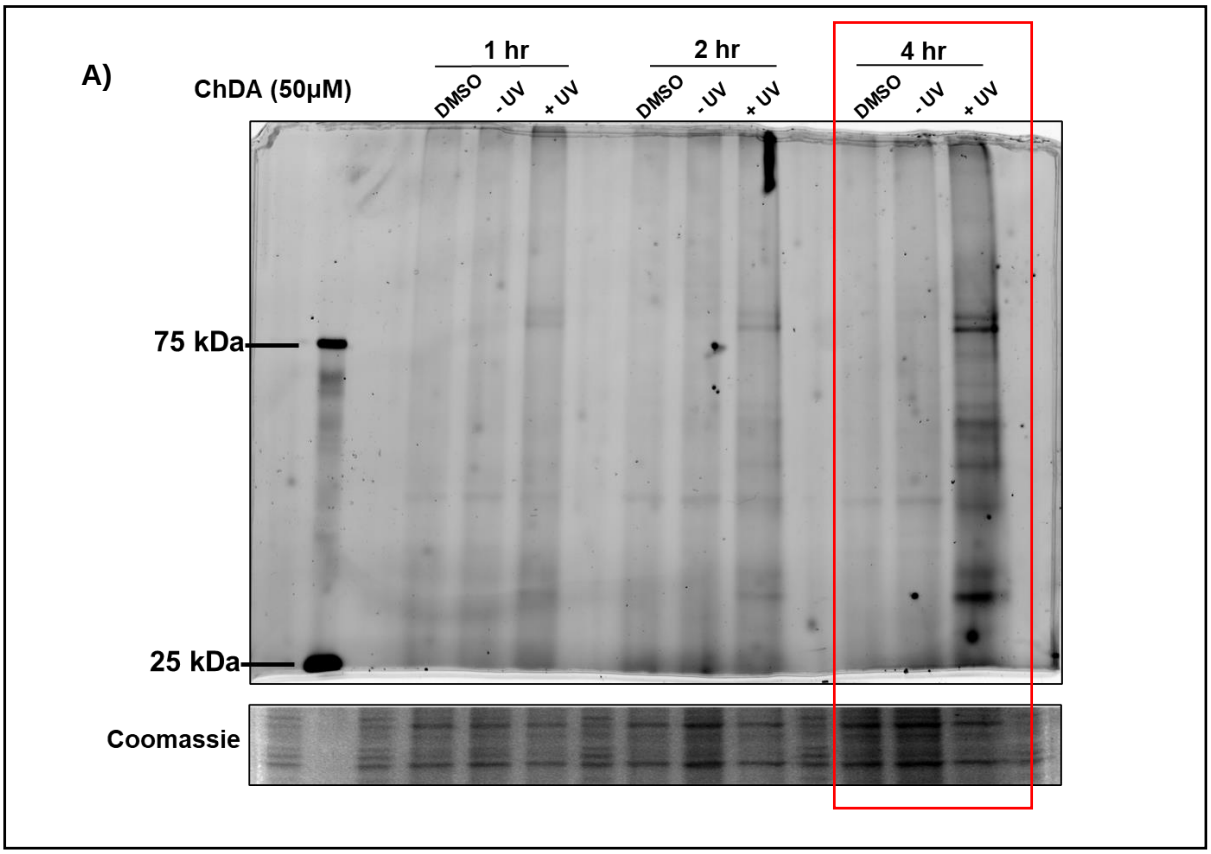

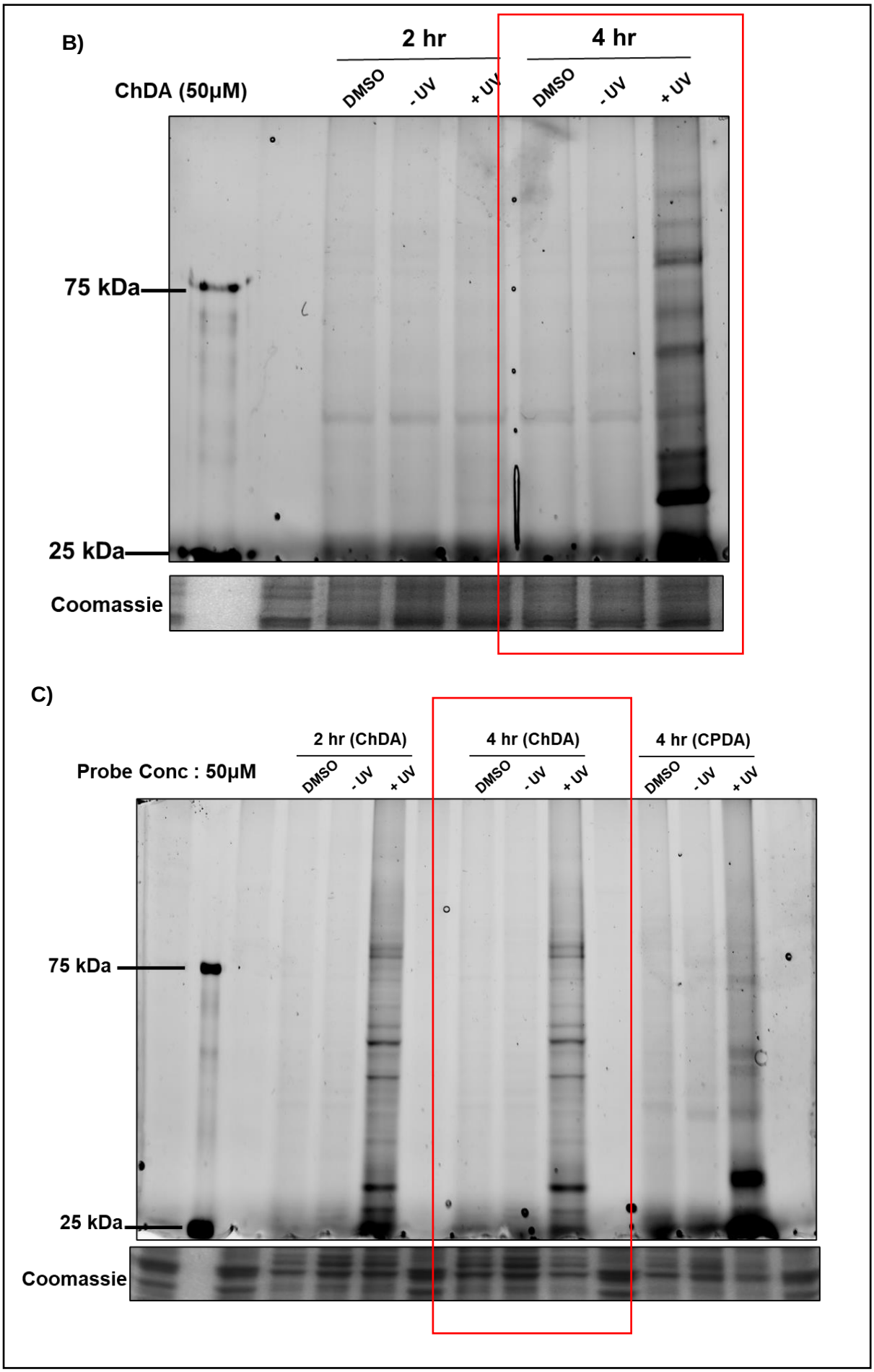
B)
2 hr
4 hr
ChDA (50μM)
DMSO
- UV
+ UV
DMSO
- UV
+ UV
75 kDa
25 kDa
Coomassie
C)
2 hr (ChDA)
4 hr (ChDA)
4 hr (CPDA)
Probe Conc : 50μM
DMSO
- UV
+ UV
DMSO
- UV
+ UV
DMSO
- UV
+ UV
75 kDa
25 kDa
Coomassie

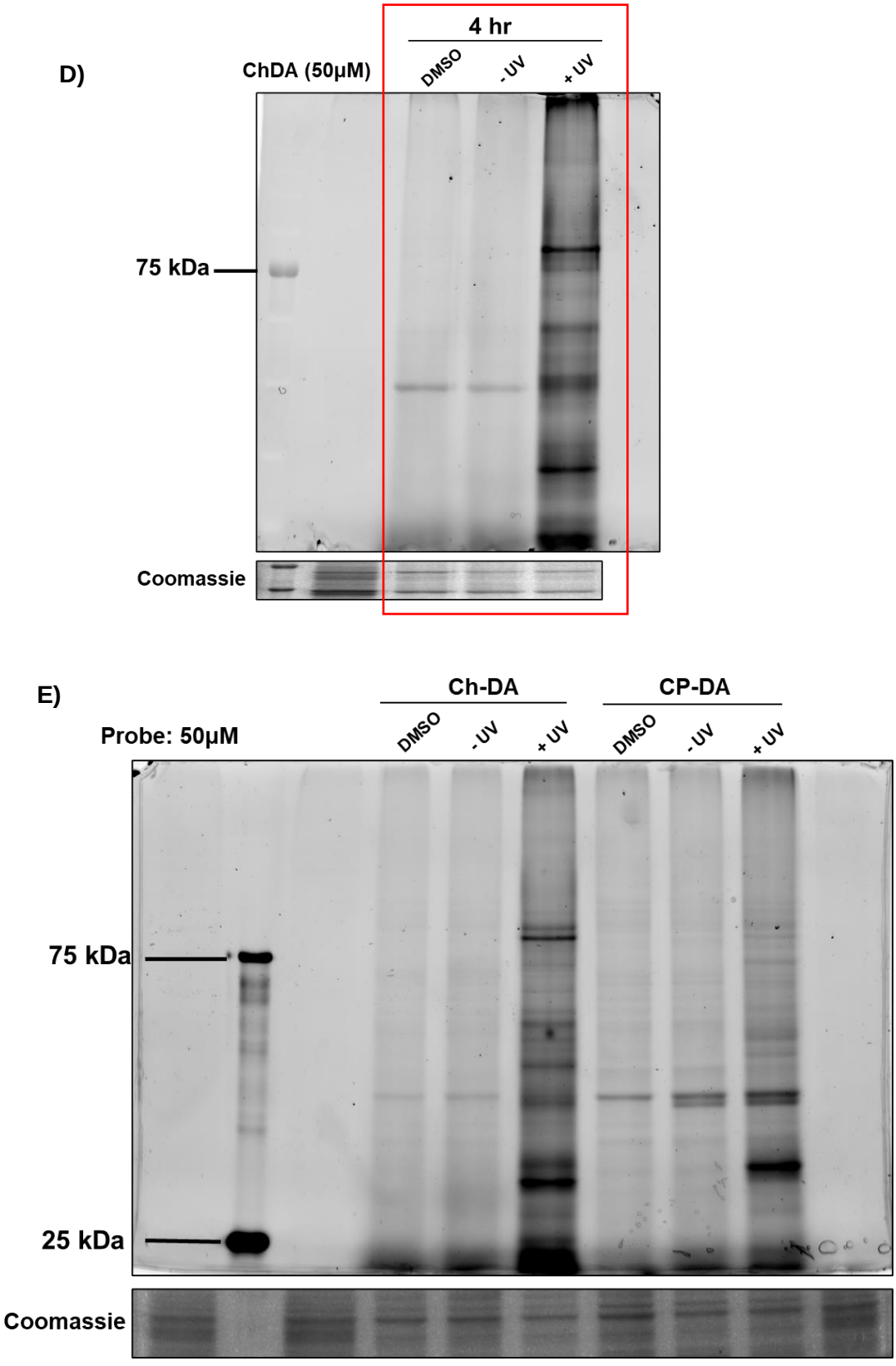

Figure 7. Optimising ChDA probe in cell lines. A-D) In-gel fluorescence for 50μM concentration at varying incubation times in RAW 264.7, N2a, BV2, and primary macrophages, respectively. C,E) Comparison of CPDA vs. ChDA probe in RAW 264.7 cell line.

3.1.3 MβCD/PBS system delivers both the probes inside cells more effectively

The use of cyclodextrins to deliver/modulate lipid levels in cells is well-established. While α-cyclodextrins have higher affinities to form complexes with phospholipids, β-cyclodextrins prefer interacting most with cholesterol. Hence, the use of β-cyclodextrins, especially methyl-β-cyclodextrin (MβCD), to deliver cholesterol into cells is well-known. However, no studies till now report the use of MβCD for the delivery of cholesteryl esters. Since cholesteryl esters are much larger in size than cholesterol, the binding affinities of these molecules with MβCD are most likely to be different, rendering it still elusive for their use as delivery agents for cholesteryl esters. In addition, even when delivering cholesterol, MβCD associated toxicities have been reported for incubation times of more than 30 min. These toxicities arise due to the complex formation of these molecules with membrane cholesterol. Now since cholesterol can possibly bind to MβCD at higher affinities than their esters, the MβCD-associted cell toxicity may occur at a higher rate when delivering cholesteryl esters, as membrane cholesterol can displace them more easily. Having said so, MβCD allows for a profoundly high increase in the solubility of sterols in polar solvents. This would also allow for a possibility of testing the probes in cell lysates. Therefore, considering both the pros and cons, we decided to evaluate the efficacy of using MβCD as a delivery agent for both the sterol probes. For this purpose, we made a 1mM stock solution containing the probe encapsulated inside MβCD in PBS, with a 1:10 ratio of probe: MβCD (materials and methods). As mentioned before, we incubated the cells with the same probe concentration as before (i.e., 50μM) and maximum for 30 min to avoid MβCD-associated toxicity. We also compared the gel profiles of MβCD delivered probes with their DMSO-delivered ones. We found that the intensity of protein bands for both probes was higher when MβCD was used (**Figure 8 A-D**). We also went ahead to test the probes in lysates. Surprisingly, the ChDA probe showed protein bands (although fewer than live-cell study), but CPDA did not (**Figure 8 E**). This could mean that the proteins interacting with CPDA may require the innate cellular environment for optimal activity. In addition to this, using gel analysis, we also found that the CPDA-MβCD complex is not very stable, lasting only around 1-2 weeks after preparation (data not shown). However, the ChDA-MβCD complex is stable, showing stability for 1-2 months. This is in line with previous reports of MβCD favouring interactions with cholesterol more. Nonetheless, both the delivery methods for both

the probes gave best results in live-cell treatment, and with similar band profiles, but with differences in intensities. Before proceeding with proteomics, it is also necessary to know whether the probes indeed enter the cells completely or are localized only on the plasma membrane due to their high lipophilicity. Hence, we proceeded to do microscopy experiments in the mentioned cell lines.

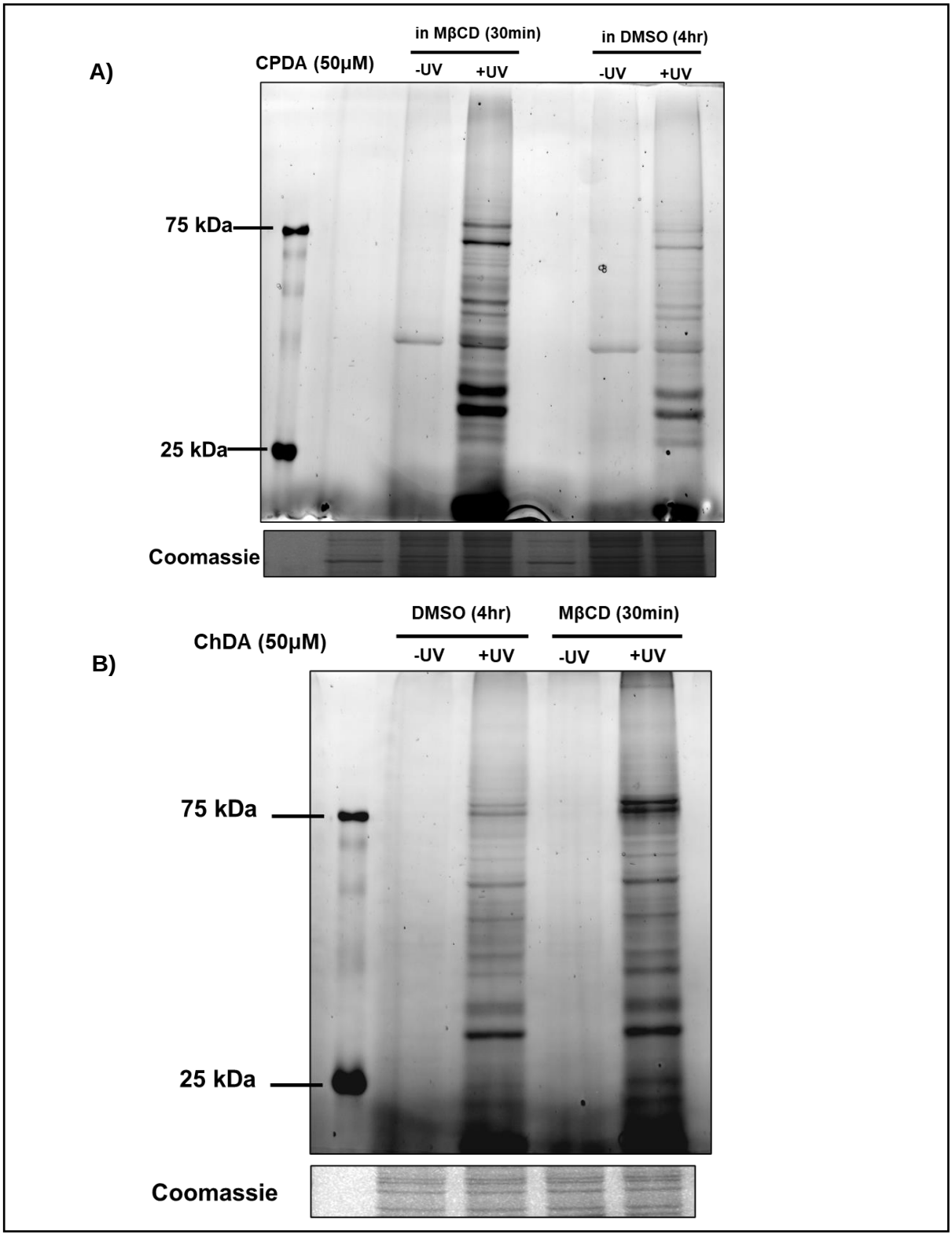

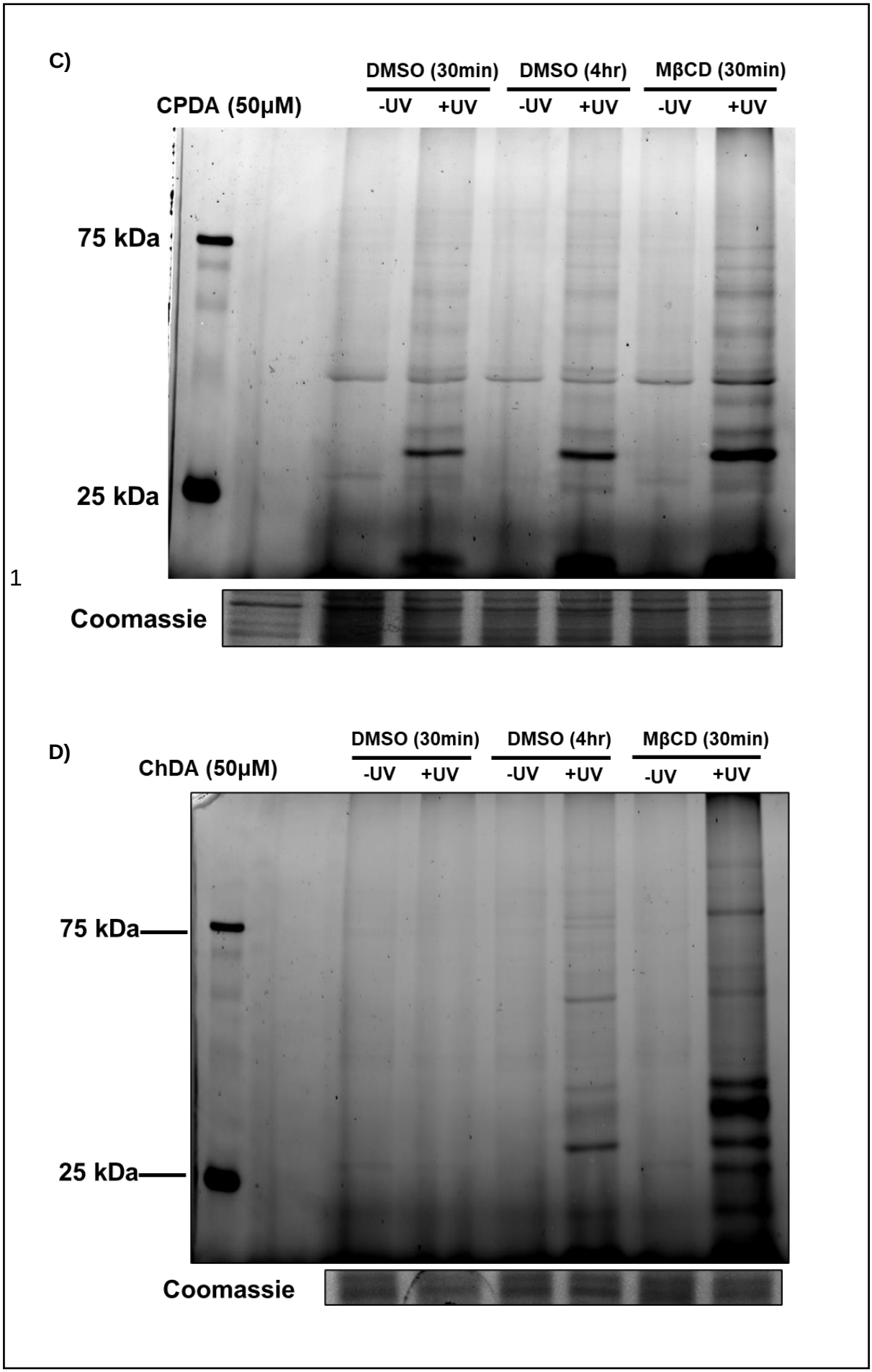
C)
DMSO (30min)
DMSO (4hr)
MβCD (30min)
CPDA (50μM)
-UV
+UV
-UV
+UV
-UV
+UV
75 kDa
25 kDa
Coomassie
D)
DMSO (30min)
DMSO (4hr)
MβCD (30min)
ChDA (50μM)
-UV
+UV
-UV
+UV
-UV
+UV
75 kDa
25 kDa
Coomassie

1

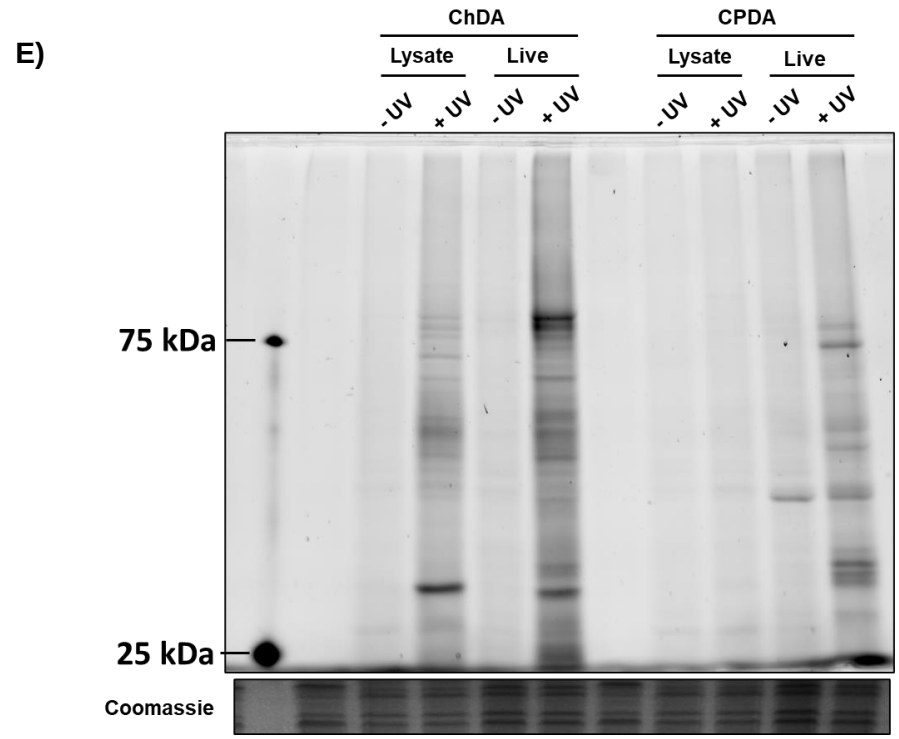

Figure 8. Delivering sterol probes in cells using methyl-β-cyclodextrin (mβCD). A, B) Comparison of DMSO vs. mβCD for CPDA and ChDA in RAW 264.7 cell line, respectively; C, D) Comparison of DMSO vs. mβCD for CPDA and ChDA, respectively in N2a cell line; E) Comparing both sterol probes in RAW 264.7 in lysates vs. live cells upon using mβCD.

3.2 Visualizing protein-probe complex inside cells

After confirming the interactions on the gels, we performed microscopy experiments to study the localization of the probe and its interacting proteins. Cells were fixed with methanol and a rhodamine tag was clicked to the probe-protein complex. As seen in **Figure 9**, only UV irradiated samples show a significant rhodamine azide intensity (RAW 264.7 cells). Any unbound probe is washed away; hence, negligible probe can be seen in the non-UV control. Interestingly, the localization of the protein-probe complex was observed to be distributed throughout the cytoplasm, with no intensity in the nucleus. Similar results were obtained in other cell lines (**Figure S1-2**). Since the lipid probe needs to be clicked with a rhodamine tag with a copper-catalysed reaction, this study was limited to fixed cells due to copper-associated toxicities. Moreover, methanol was chosen for fixing cells as other fixatives like paraformaldehyde (PFA) would cross-link the probe-protein complex irrespective of UV irradiation. All in all, these results suggest that these protein interactions are indeed on a pan-cellular scale and are not limited to plasma membrane proteins.

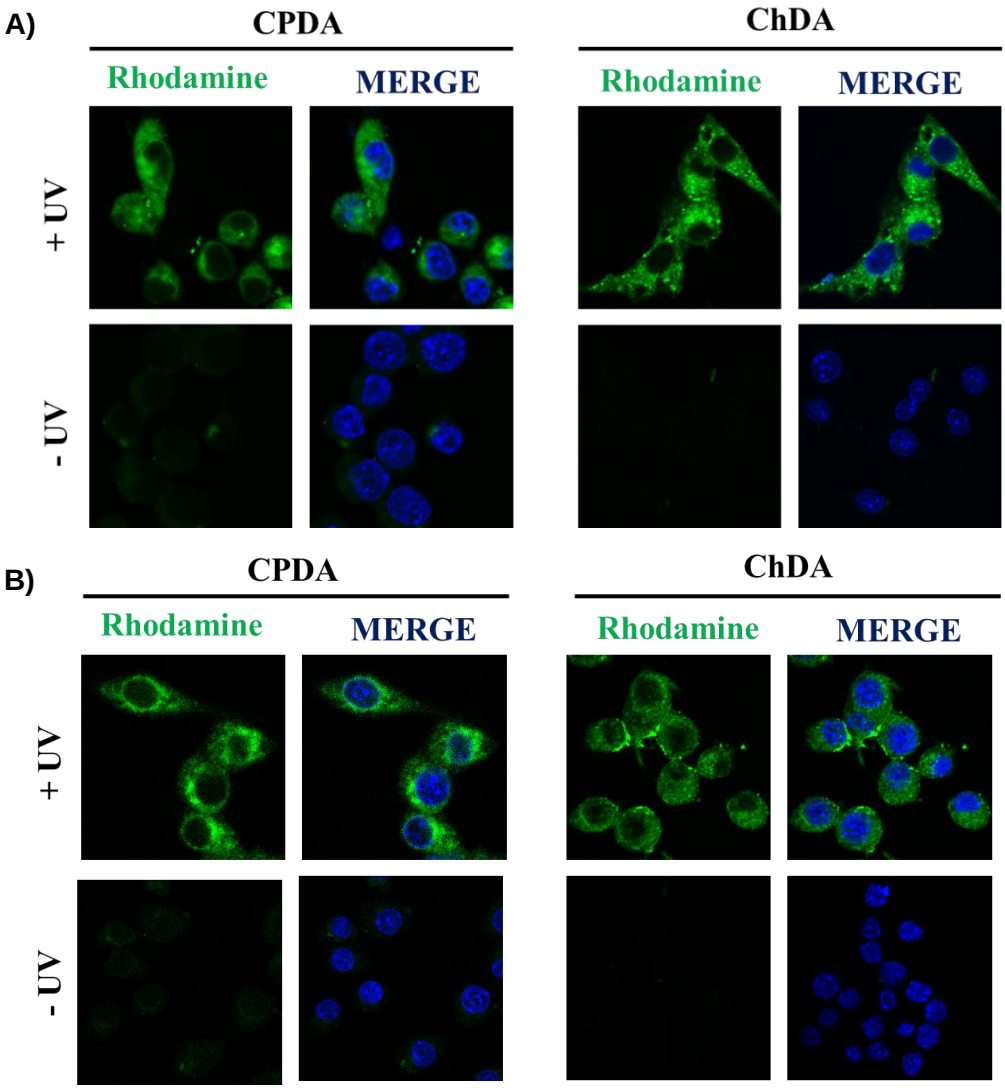

Figure 9. Visualization of probe-protein complex inside cells (RAW 264.7). A) Using DMSO; and B) using MβCD. The green signal corresponds to rhodamine intensity, while the blue indicates nuclear staining due to DAPI binding.

3.3 Quantifying probe uptake by cells

To estimate the amount of probe entering inside cells, we performed lipidomics analysis on cells (RAW 264.7 and N2a) after incubating them with the probe. The samples were analysed in positive mode in a LC-ESI-QTOF instrument. We looked for the most possible ionizable versions of both the probes (H^+, NH_4^+). While CPDA probe was detected in cells at a considerable amount, ChDA probe was not detected in significant quantities. Since the internal standard was detected fine, we speculated whether the probes were not getting ionised suitably. While cholesterol is usually

ionised by dehydration of 3’ hydroxy group in ESI-MS experiments, the ether linkage in ChDA probe perhaps renders it difficult to be ionised. Due to this reason, ChDA was not detected at appreciable quantities. It should also be noted that this experiment is at-best semi-quantitative, and a more detailed analysis for accurate quantification of the probes needs to be done. For example, a targeted triple-quadrupole based method using a standard curve should be used for better quantification. Having said so, since the earlier evidence obtained by gel experiments and microscopy confirms the probe uptake, we decided to proceed with proteomics experiments to identify the initial protein hits of these probes.

3.4 Proteomics

After optimizing the probe usage conditions in the cell lines of interest for both the probes, we proceeded to identify the interacting proteins. This was done by clicking the probe with biotin-azide, and isolating the probe-protein complex using avidin beads. The proteins were digested using trypsin, and the generated peptides from control (-UV) and (+UV) were differentially labelled using reductive dimethylation labelling. This differential labelling is important to identify proteins getting enriched in particular samples, and by taking a higher Heavy to Light (H/L) ratio, we can identify proteins specific to the +UV sample (considering that we label +UV samples with heavy label). This helps in filtering the proteins that show non-specific binding in the control samples. To identify the interactors, the following filtering criteria was used: the identified proteins must be present in at least two out of three replicates, the identified protein must have at least 99% match to the compared protein in the library, minimum peptide count detected should be three, and heavy to light ratio should be at least 1.5. Theoretically, H/L ratio equal to one indicates equal enrichment in test (+UV) vs. control (-UV), H/L greater than one indicates enrichment in +UV, while H/L lower than one is an indication of enrichment in -UV samples. We hence put a threshold of H/L ≥ 1.5, to identify enrichment in +UV samples. The proteomics procedure was first tested in two cell lines: RAW 264.7 and N2a. During initial stages, very few peptides were detected after the mass spectrometry runs (**Figure S3A**). Due to this, we decided to increase the protein concentration used for the proteomics procedure, which meant more protein amount was submitted for mass spectrometry runs (initial protein

concentration was increased from 500 μg/mL to 1 mg/mL). Along with this, we also increased the avidin bead incubation time from 1.5 hour to 2.5 hours, to allow for better enrichment. This was tested with the N2a cell line with both probes in DMSO-mediated delivery, as well as for CPDA probe with MβCD-mediated delivery. This time, we could obtain better spectral counts as compared to previous analysis (**Figure S3B**). For the CPDA probe (in DMSO) samples, around 600 proteins were detected, out of which around 450 proteins had peptide counts greater than 3. After filtering H/L ratio, around 23 proteins were left. For this experiment, since only 2 replicates were run till now, we filtered the common proteins identified between them. **Figure 10** shows these identified interactors.

Similarly, for ChDA probe in DMSO in N2a cell line, total number of proteins detected were around 600. After filtering with the mentioned criteria, around 28 proteins remained. For this experiment, since only 2 replicates were run till now, we filtered the common proteins identified between them. **Figure 11** shows the top hits of these identified interactors.

We also tested both the sterol probes in N2a cells when delivered using MβCD vehicle. The total proteins detected for CPDA were around 500 in three replicates. However, we could only detect 300 proteins for the ChDA probe. Post filtering, the protein hits identified for both the probes are given in **Figures 12 and 13**. For CPDA, 41 proteins were identified, whereas for ChDA, 22 proteins were identified.

The CPDA probe was also tested in RAW 264.7 cells, however at around 0.4 mg/mL of total protein concentration. Compared to N2a which did not give appreciable spectral counts at even 0.5 mg/mL, we could obtain around 37 thousand spectral counts for RAW 264.7 cells after the mass spectrometry runs (data not shown). From this, around 150 proteins were detected in each of the three replicates. The final hits obtained from these analyses are given in **Figure 14**.

A)

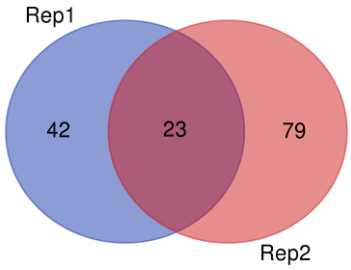

B)

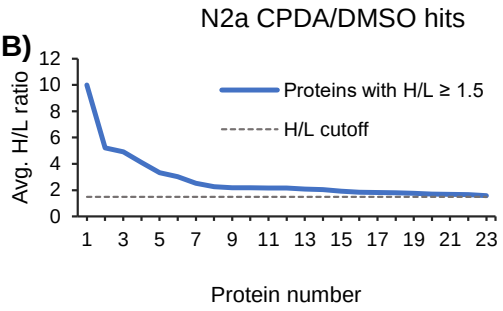

C)

Protein name [Mus musculus]	Avg. H/L
embigin precursor	46.54
voltage-dependent anion-selective channel protein 1 isoform 2	5.22
saccharopine dehydrogenase-like oxidoreductase	4.91
voltage-dependent anion-selective channel protein 2	4.11
transgelin-2	3.33
protein transport protein Sec61 subunit alpha isoform 1	3.03
sodium/potassium-transporting ATPase subunit alpha-1	2.53
heterogeneous nuclear ribonucleoprotein A/B isoform 2	2.25
NADH-cytochrome b5 reductase 3 isoform X1	2.19
very-long-chain enoyl-CoA reductase isoform 1	2.19
NADPH--cytochrome P450 reductase	2.16
oxygen-dependent coproporphyrinogen-III oxidase, mitochondrial precursor	2.16
far upstream element-binding protein 3 isoform b	2.08
ADP/ATP translocase 1	2.05
dolichyl-diphosphooligosaccharide--protein glycosyltransferase subunit 1 precursor	1.92
transducin beta-like protein 3	1.85
sphingosine-1-phosphate lyase 1	1.82
nuclear pore complex protein Nup160 isoform X1	1.79
delta(14)-sterol reductase LBR isoform X1	1.76
calnexin precursor	1.71
vimentin	1.68
heterogeneous nuclear ribonucleoprotein H isoform X8	1.67
sarcoplasmic/endoplasmic reticulum calcium ATPase 2 isoform b	1.59

D)

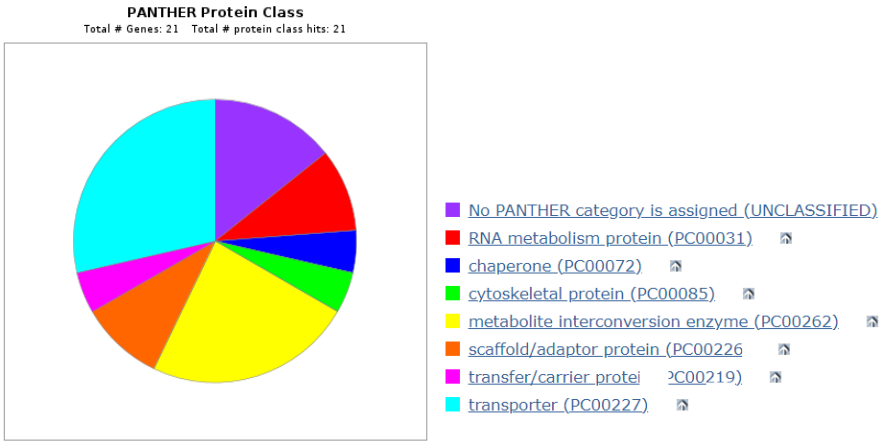

Figure 10. Initial protein hits with CPDA probe (in DMSO) in N2a cell line. A) Venn diagram showing proteins obtained in two replicates (*source: bioinformatics and Evolutionary Genomics\Venn*) B) Proteins with H/L ≥ 1.5. C) Identified protein hits with their average H/L ratios D) Classification of identified proteins based on their cellular function (*source: Panther Database*).

A)

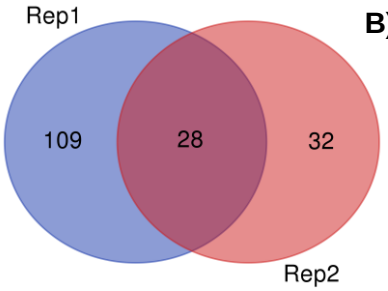

B)

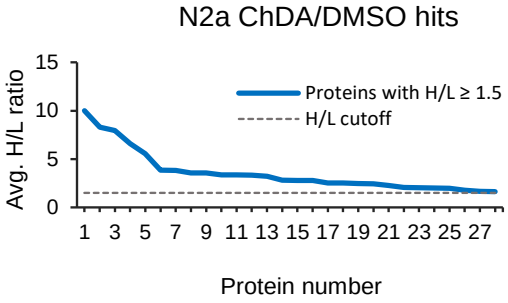

C)

Protein Name [Mus musculus]	Avg. H/L
high mobility group protein B2	12.12
serine/arginine-rich splicing factor 6	8.29
60S ribosomal protein L7	7.94
elongation factor 1-gamma	6.58
myb-binding protein 1A	5.54
voltage-dependent anion-selective channel protein 2	3.84
nucleolar RNA helicase 2	3.81
heat shock protein HSP 90-alpha	3.57
60S ribosomal protein L22 isoform a	3.56
non-POU domain-containing octamer-binding protein	3.37
T-complex protein 1 subunit gamma	3.36
histone H3.1	3.33
histone H2A type 2-C	3.21
plasma membrane calcium-transporting ATPase 1 isoform X2	2.81
60S ribosomal protein L31	2.8
serine/arginine-rich splicing factor 5 isoform X1	2.8
40S ribosomal protein S24 isoform 3	2.53
igE-binding protein-like, partial	2.52
heterogeneous nuclear ribonucleoprotein L isoform X1	2.46
60S ribosomal protein L13a	2.44
peptidyl-prolyl cis-trans isomerase A	2.28
voltage-dependent anion-selective channel protein 1 isoform 2	2.07
histone H2A type 1-B	2.02
matrin-3	2.01
60S ribosomal protein L4	1.97
rRNA 2'-O-methyltransferase fibrillarin	1.78
delta(14)-sterol reductase LBR isoform X1	1.66
40S ribosomal protein S23	1.64

D)

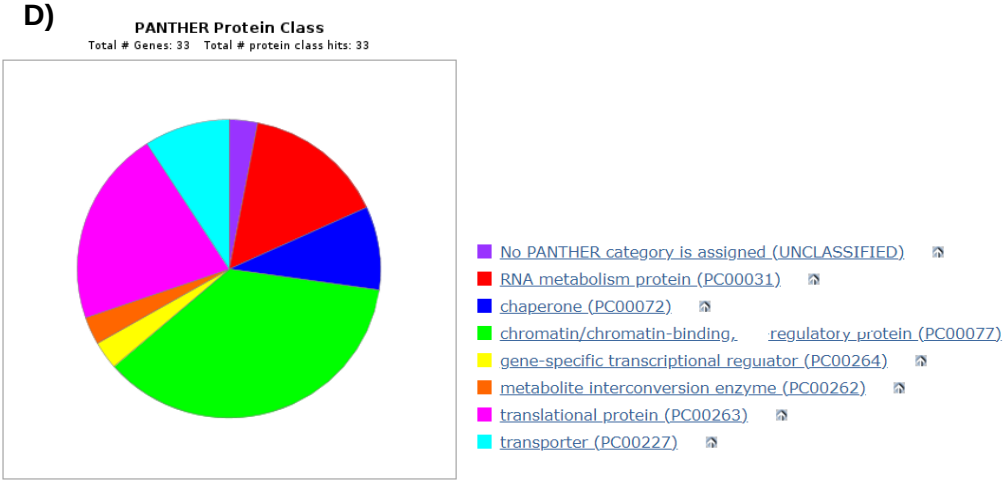

Figure 11. Initial protein hits with ChDA probe (in DMSO) in N2a cell line. A) Venn diagram showing proteins obtained in two replicates B) Proteins with H/L ≥ 1.5. C) Identified protein hits with their average H/L ratios D) Classification of identified proteins based on their cellular function.

A)

Protein Name [Mus musculus]	Avg. H/L
60S ribosomal protein L18	10.51
voltage-dependent anion-selective channel protein 1 isoform 2	8.84
ADP/ATP translocase 2	8.76
NADH-cytochrome b5 reductase 3 isoform X1	7.05
histone H3.2	6.18
keratin Kb40 isoform X2	5.18
keratin, type II cytoskeletal 2 epidermal isoform X1	4.89
voltage-dependent anion-selective channel protein 2	4.45
dolichyl-diphosphooligosaccharide--protein glycosyltransferase subunit STT3A	4.27
saccharopine dehydrogenase-like oxidoreductase	4.09
histone H1.1	3.2
keratin, type II cytoskeletal 1	3.12
igE-binding protein-like	3.11
dolichyl-diphosphooligosaccharide--protein glycosyltransferase subunit 2 isoform X1	2.94
voltage-dependent anion-selective channel protein 3 isoform 2	2.53
dehydrogenase/reductase SDR family member 1	2.49
histone H1.4	2.47
histone H2AX	2.47
NADPH--cytochrome P450 reductase	2.35
histone H1.5	2.24
ADP-dependent glucokinase isoform 1 precursor	2.2
heat shock protein 75 kDa, mitochondrial precursor	2.06
H2b histone family, member A isoform 2	2.06
60 kDa heat shock protein, mitochondrial	2.04
keratin, type II cytoskeletal 5	2.02
histone H4	2.01
40S ribosomal protein S13	1.85
40S ribosomal protein S8	1.84
protein disulfide-isomerase A3 precursor	1.79
ribosomal L1 domain-containing protein 1	1.75
heterogeneous nuclear ribonucleoprotein U isoform X2	1.74
vimentin	1.74
ATP synthase subunit alpha, mitochondrial precursor	1.74
transgelin-2	1.72
heterogeneous nuclear ribonucleoprotein Q isoform 3	1.7
dolichyl-diphosphooligosaccharide--protein glycosyltransferase subunit 1 precursor	1.68
nucleolar protein 56	1.67
interleukin enhancer-binding factor 3 isoform X10	1.67
U5 small nuclear ribonucleoprotein 200 kDa helicase	1.64
GTP-binding protein 4	1.56
endoplasmin precursor	1.53

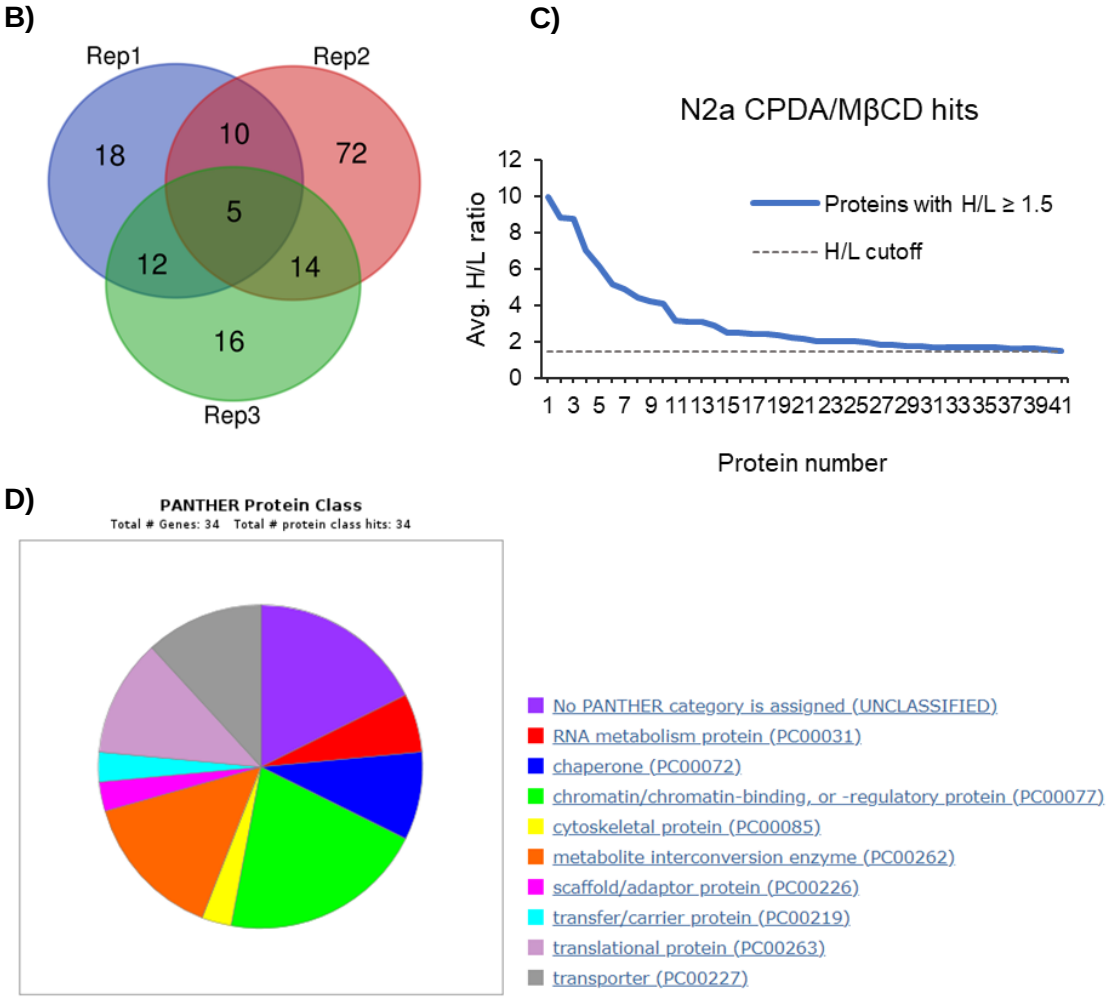

Figure 12. Initial protein hits with CPDA probe (in MβCD) in N2a cell line. A) Identified protein hits with their average H/L ratios B) Venn diagram showing proteins obtained in two replicates C) Proteins with H/L ≥ 1.5. D) Classification of identified proteins based on their cellular function.

A)

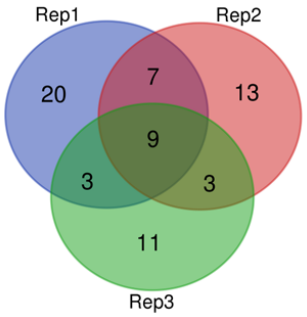

B)

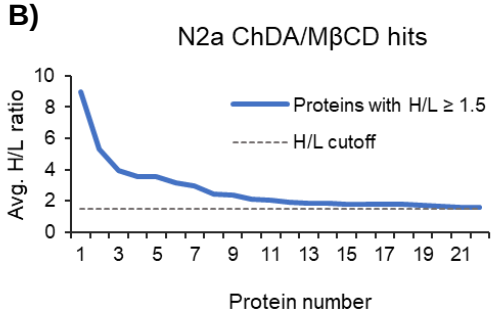

C)

Protein name	Avg. H/L
sodium/potassium-transporting ATPase subunit alpha-1 [Mus musculus]	8.99
voltage-dependent anion-selective channel protein 1 isoform 2 [Mus musculus]	5.34
guanine nucleotide-binding protein G(I)/G(S)/G(T) subunit beta-1 [Mus musculus]	3.96
ADP/ATP translocase 2 [Mus musculus]	3.58
calnexin precursor [Mus musculus]	3.54
nucleolin [Mus musculus]	3.16
voltage-dependent anion-selective channel protein 2 [Mus musculus]	2.96
plasma membrane calcium-transporting ATPase 1 isoform X2 [Mus musculus]	2.42
histone H1.5 [Mus musculus]	2.41
thioredoxin-related transmembrane protein 1 precursor [Mus musculus]	2.13
ADP/ATP translocase 1 [Mus musculus]	2.04
H2b histone family, member A isoform 2 [Mus musculus]	1.89
4F2 cell-surface antigen heavy chain isoform b [Mus musculus]	1.86
heterogeneous nuclear ribonucleoprotein H isoform X8 [Mus musculus]	1.85
histone H1.2 [Mus musculus]	1.81
vimentin [Mus musculus]	1.81
nucleoporin NDC1 [Mus musculus]	1.79
phosphate carrier protein, mitochondrial precursor [Mus musculus]	1.77
histone H1.1 [Mus musculus]	1.74
60S ribosomal protein L22 isoform a [Mus musculus]	1.64
delta(14)-sterol reductase LBR isoform X1 [Mus musculus]	1.62
60 kDa heat shock protein, mitochondrial [Mus musculus]	1.6

D)

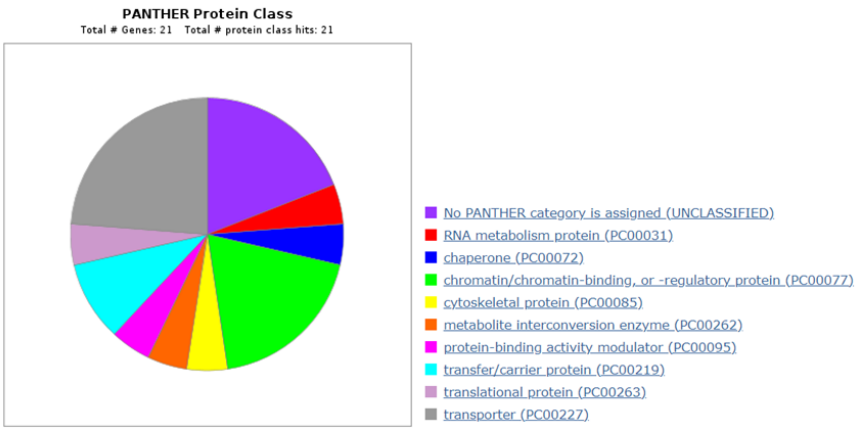

Figure 13. Initial protein hits with ChDA probe (in MβCD) in N2a cell line. A) Venn diagram showing proteins obtained in two replicates B) Proteins with H/L ≥ 1.5. C) Identified protein hits with their average H/L ratios D) Classification of identified proteins based on their cellular function.

A)

B)

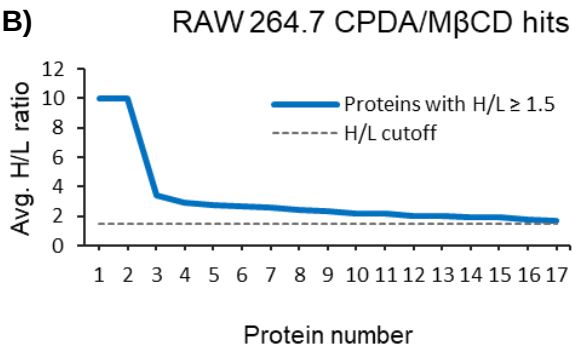

C)

Protein Name [Mus musculus]	Avg. H/L
voltage-dependent anion-selective channel protein 2	13.81
voltage-dependent anion-selective channel protein 1 isoform 2	12.16
splicing factor, proline- and glutamine-rich	3.41
heterogeneous nuclear ribonucleoproteins A2/B1 isoform X1	2.92
malate dehydrogenase, mitochondrial precursor	2.73
stress-70 protein, mitochondrial	2.65
histone H3.2	2.57
prelamin-A/C isoform X1	2.39
serine/arginine-rich splicing factor 3	2.35
non-POU domain-containing octamer-binding protein	2.21
histone H1.4	2.18
neutral alpha-glucosidase AB isoform 1	2.02
protein disulfide-isomerase A3 precursor	1.98
ATP synthase subunit beta, mitochondrial precursor	1.95
ubiquitin-40S ribosomal protein S27a precursor	1.9
eukaryotic initiation factor 4A-I isoform 1	1.81
60S ribosomal protein L13	1.72

D)

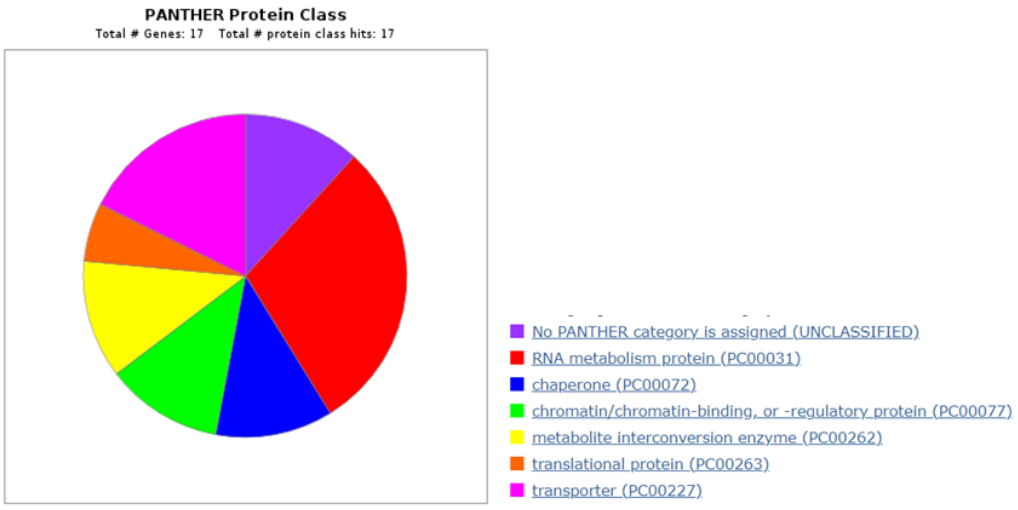

Figure 14. Initial protein hits with CPDA probe (in MβCD) in RAW 264.7 cell line. A) Venn diagram showing proteins obtained in two replicates B) Proteins with H/L ≥ 1.5. C) Identified protein hits with their average H/L ratios D) Classification of identified proteins based on their cellular function.

Chapter 4 Discussion and Future Directions

Lipid-protein interactions have emerged as an interesting area in the field of macromolecular interactions. However, identification of the protein interactome of lipids has remained challenging. Our study provides chemical biology-based evidence to identify these interactors of a so far less studied class of lipids: cholesteryl esters.

We show that the synthesized bioorthogonal probes, both cholesteryl ester and cholesterol, are capable of binding to and pulling down the interacting proteins. These probes can be efficiently used in numerous cell lines, and can be therefore be used to compare the cell-type specific interactomes. In our study, we found evidence that macrophagic, and cells of neural origin efficiently take up the probe and show a difference in the protein interactors (both in terms of quantity and type of protein identified), as analysed by in-gel fluorescence analysis and proteomics. This is in line with the previous reports on the activity of cholesteryl esters in immune and neural cells, while other cells (e.g., from kidney) did not show much of an activity under normal cell conditions. Future studies can also attempt using the probe in cancer cell lines (e.g., Hela and A549) to check if cancers have a distinct set of proteins interacting. From the in-gel fluorescence analysis, it is clear that both the probes show considerable difference in the protein band pattern seen, which hints to differences in their interactome. It is not surprising that cholesterol probe interacts more proteins on gel in all the cell lines as the role of cholesterol is fairly diverse inside cells, compared to their esters. Apart from this, there are some non-specific bands also visible in the gels. For example, the vehicle-control lane also shows a clear band, which appears in all the cell lines. This could be an artifact of the click reaction, or an unknown protein interacting with rhodamine. This non-specific background would however be eliminated during comparison of -UV and +UV in proteomics, hence the final proteins identified will all be specific to the probe.

Our study also adds to the existing data of utilising different methodologies to deliver highly lipophilic molecules in different cell lines, and this is the first study that provides strategies for lipoprotein independent delivery of cholesteryl esters into cells. While the type of proteins interacting does not seem to change when analysed in gels between two delivery methods (since we do not see a major change in the band

pattern of the gels between two delivery methods (except for intensity)), our proteomics data hints at minor differences that may arise due to the efficiency of delivery by the vehicle itself. Apart from this, translation of these studies into animal tissues would be ideal to support the results obtained in cell lines. Since working with organ lysates for validating the above is one of the easier ways of verification, not being able to work with lysates with cholesteryl ester probe may offer a challenge. Hence, future studies can test to better solubilise the cholesteryl ester probe either by changing the ratio from 1:10 to 1:20 (probe: cyclodextrin), or by using other members of cyclodextrins, like the gamma cyclodextrin (since it has bigger cavity and better solubility in water), and test if it makes the probe feasible for lysate studies.

The microscopy data highlights that the probe reaches over completely to the cytoplasmic region. It would be interesting to see in future if this co-localises to some organelles more and then compare it with the proteins identified in proteomics. For example, a protein in lipid droplets may interact with the probe and this may be visualised using a lipid-droplet marker. Apart from this, it should also be noted that since copper catalysed click chemistry is not amenable for live cell studies, visualising the kinetics of the probe uptake was not possible in this study.

In the proteomics data obtained for N2a cells, both the probes in both delivery methods show differences in the identified initial hits. However, in the experiments carried out thus far, we noticed that the ReDiMe labelling was not optimum and hence much lesser proteins could meet the filtering criteria. Future work should focus on either increasing the ReDiMe reaction time (from 1 to 2hr), or changing the labelling from 4% to 8%. From the proteomics analysis thus far, we could identify protein hits that are known lipid interactors (for eg. very-long-chain enoyl-CoA reductase), suggesting that the probe indeed mimics a lipid. Furthermore, known sterol interactors (for eg. delta(14)-sterol reductase LBR, which is involved in cholesterol biosynthesis), were identified with both the sterol probes, which suggests that the probes mimic the natural cellular sterols. To note, three proteins (saccharopine dehydrogenase-like oxidoreductase, transgelin-2, and dolichyl-diphosphooligosaccharide--protein glycosyltransferase subunit 1 precursor) were identified in CPDA probe in both the vehicles. Interestingly, saccharopine dehydrogenase-like oxidoreductase is present in the lipid droplets, and it is therefore possible that it may interact with cholesteryl esters. It is interesting to note that IgE-binding protein was detected in ChDA (in DMSO) and also in CPDA (in

mβCD). However, the H/L ratio in CPDA was slightly higher than ChDA (3.11 vs. 2.52). It would be important to do competition experiments in future to identify if this protein prefers binding to either of the probes. Proteomics with ChDA probe in mβCD in RAW 264.7 needs to be done, and further competition experiments, both with ChDA and PADA, need to be carried out in both cell lines. This will help screening of the found protein hits and identify the specific interactors. After screening of these hits, validation of these interactors by overexpressing them in respective cell lines would also be of interest in the future.

Lastly, our data shows usage of the probe in healthy cells, however, the probe can also be tested in future studies in cells with oxidative stress or high cholesterol stress conditions. This will also help recapitulate cellular signalling during disease conditions and we can compare any changes in the interactome with its healthy state. In addition, it should also be noted that our probe is a racemic mixture of all the enantiomers and the exact active compound is still unknown. The proteins, most likely, would be stereoselective and hence the active enantiomer could be found in future studies. Once purification of enantiomers is possible, it can also be crystallised to see which one resembles more to cholesteryl palmitate, which is the natural interactor to these proteins.

References

Alberts, B, Johnson, A, Lewis, J, Raff, M, Roberts, K, and Walter, P (2002). The lipid bilayer. Molecular Biology of the Cell - NCBI Bookshelf. Available at: https://www.ncbi.nlm.nih.gov/books/NBK26871/.

Allen, WV (1976). Biochemical aspects of lipid storage and utilization in animals. American Zoologist 16, 631–647.

Ansell, TB, Curran, L, Horrell, MR, Pipatpolkai, T, Letham, SC, Song, W, Siebold, C, Stansfeld, PJ, Sansom, MSP, and Corey, RA (2021). Relative Affinities of Protein–Cholesterol Interactions from Equilibrium Molecular Dynamics Simulations. Journal of Chemical Theory and Computation 17, 6548–6558.

Bieberich, E (2008). Ceramide signaling in cancer and stem cells. Future Lipidology 3, 273–300.

Chang, TY, Chang, CCY, Harned, TC, De La Torre, AL, Lee, J, Huynh, TNT, and Gow, JG (2021). Blocking cholesterol storage to treat Alzheimer's disease. Exploration of Neuroprotective Therapy 1, 173–184.

Choi, SH, Sviridov, D, and Miller, YI (2017). Oxidized cholesteryl esters and inflammation. Biochimica Et Biophysica Acta (BBA) - Molecular and Cell Biology of Lipids 1862, 393–397.

Christian, AE, Haynes, MP, Phillips, MC, and Rothblat, GH (1997). Use of cyclodextrins for manipulating cellular cholesterol content. Journal of Lipid Research 38, 2264–2272.

Click Chemistry. Available at: https://www.organic-chemistry.org/namedreactions/click-chemistry.shtm.

Cutler, RG, Pedersen, WA, Camandola, S, Rothstein, JD, and Mattson, MP (2002). Evidence that accumulation of ceramides and cholesterol esters mediates

oxidative stress–induced death of motor neurons in amyotrophic lateral sclerosis. Annals of Neurology 52, 448–457.

Deamer, DW (2017). The role of lipid membranes in life's origin. Life 7, 5.

Dowhan, W, and Bogdanov, M (2002). Chapter 1 Functional roles of lipids in membranes. In: New Comprehensive Biochemistry, 1–35.

Dufourc, ÉJ (2008). Sterols and membrane dynamics. Journal of Chemical Biology 1, 63–77.

Escribá, PV, Wedegaertner, P, Goñi, FM, and Vögler, O (2007). Lipid–protein interactions in GPCR-associated signaling. Biochimica Et Biophysica Acta (BBA) - Biomembranes 1768, 836–852.

Fielding, CJ, and Fielding, PE (1982). Cholesterol transport between cells and body fluids: role of plasma lipoproteins and the plasma cholesterol esterification system. Medical Clinics of North America 66, 363–373.

Ghosh, S, Zhao, B, Bie, J, and Song, J (2010). Macrophage cholesteryl ester mobilization and atherosclerosis. Vascular Pharmacology 52, 1–10.

Glomset, JA (1962). The mechanism of the plasma cholesterol esterification reaction: Plasma fatty acid transferase. Biochimica Et Biophysica Acta 65, 128–135.

Gubbens, J, and De Kroon, AIPM (2010). Proteome-wide detection of phospholipid–protein interactions in mitochondria by photocrosslinking and click chemistry. Molecular BioSystems 6, 1751.

Haldón, E, Nicasio, MC, and Pérez, PJ (2015). Copper-catalysed azide–alkyne cycloadditions (CuAAC): an update. Organic and Biomolecular Chemistry 13, 9528–9550.

Hulce, JJ, Cognetta, AB, Niphakis, MJ, Tully, SE, and Cravatt, BF (2013a). Proteome-wide mapping of cholesterol-interacting proteins in mammalian cells. Nature Methods 10, 259–264.

Katan, M, and Cockcroft, S (2020). Phosphatidylinositol(4,5)bisphosphate: diverse functions at the plasma membrane. Essays in Biochemistry 64, 513–531.

Leitinger, N (2003). Cholesteryl ester oxidation products in atherosclerosis. Molecular Aspects of Medicine 24, 239–250.

Li, J, Gu, D, Lee, SSY, Song, B-L, Bandyopadhyay, S, Chen, S, Konieczny, SF, Ratliff, TL, Liu, X, Xie, J, *et al.* (2016). Abrogating cholesterol esterification suppresses growth and metastasis of pancreatic cancer. Oncogene 35, 6378–6388.

Li, T, and Chiang, JYL (2009). Regulation of bile acid and cholesterol metabolism by PPARs. Ppar Research 2009, 1–15.

Liu, Z, Gómez, CR, Espinoza, I, Le, T, Shenoy, V, and Zhou, X (2022). Correlation of cholesteryl ester metabolism to pathogenesis, progression and disparities in colorectal Cancer. Lipids in Health and Disease 21.

Luo, J, Yang, H, and Song, B-L (2019). Mechanisms and regulation of cholesterol homeostasis. Nature Reviews Molecular Cell Biology 21, 225–245.

Mannaerts, GP, Van Veldhoven, PP, and Casteels, M (2000). Peroxisomal Lipid Degradation via β and β-oxidation in Mammals. Cell Biochemistry and Biophysics 32, 73–87.

Marsh, D (2010). Liquid-ordered phases induced by cholesterol: A compendium of binary phase diagrams. Biochimica Et Biophysica Acta (BBA) - Biomembranes 1798, 688–699.

Martin, TFJ (2012). Role of PI(4,5)P2 in vesicle exocytosis and membrane fusion. In: Sub-Cellular Biochemistry, 111–130.

Niphakis, MJ, Lum, KM, Cognetta, AB, Correia, BE, Ichu, T-A, Olucha, J, Brown, SJ, Kundu, S, Piscitelli, F, Rosen, H, *et al.* (2015). A Global Map of Lipid-Binding Proteins and their ligandability in cells. Cell 161, 1668–1680.

Nomura, DK, and Casida, JE (2016). Lipases and their inhibitors in health and disease. Chemico-Biological Interactions 259, 211–222.

Phillips, GR, Hancock, S, Brown, SHJ, Jenner, A, Kreilaus, F, Newell, KA, and Mitchell, TW (2020). Cholesteryl ester levels are elevated in the caudate and putamen of Huntington's disease patients. Scientific Reports 10.

Pp, R (2001). Ceramide regulates cellular homeostasis via diverse stress signaling pathways. Leukemia 15, 1153–1160.

Proitsi, P, Kim, M, Whiley, L, Pritchard, M, Leung, R, Soininen, H, Kłoszewska, I, Mecocci, P, Tsolaki, M, Vellas, B, *et al.* (2015). Plasma lipidomics analysis finds long chain cholesteryl esters to be associated with Alzheimer's disease. Translational Psychiatry 5, e494.

Reza, JZ, Doosti, M, Salehipour, M, Packnejad, M, Mojarrad, M, Heidari, M, and Emamian, ES (2009). Modulation Peroxisome Proliferators Activated Receptor alpha (PPAR α) and Acyl Coenzyme A: Cholesterol Acyltransferase1 (ACAT1) Gene expression by Fatty Acids in Foam cell. Lipids in Health and Disease 8.

Rowland, MM, Bostic, HE, Gong, D, Speers, AE, Lucas, N, Cho, W, Cravatt, BF, and Best, MD (2011). Phosphatidylinositol 3,4,5-Trisphosphate activity probes for the labeling and proteomic characterization of protein binding partners. Biochemistry 50, 11143–11161.

Sakai, K, Igarashi, M, Yamamuro, D, Ohshiro, T, Nagashima, S, Takahashi, M, Enkhtuvshin, B, Sekiya, M, Okazaki, H, Osuga, J-I, *et al.* (2014). Critical role of neutral cholesteryl ester hydrolase 1 in cholesteryl ester hydrolysis in murine macrophages. Journal of Lipid Research 55, 2033–2040.

Schulz, H (1991). Beta oxidation of fatty acids. Biochimica Et Biophysica Acta 1081, 109–120.

Shanbhag, K, Sharma, K, and Kamat, SS (2023). Photoreactive bioorthogonal lipid probes and their applications in mammalian biology. RSC Chemical Biology 4, 37–46.

Stith, JL, Velazquez, FN, and Obeid, LM (2019). Advances in determining signaling mechanisms of ceramide and role in disease. Journal of Lipid Research 60, 913–918.

Sunshine, H, and Iruela-Arispe, ML (2017). Membrane lipids and cell signaling. Current Opinion in Lipidology 28, 408–413.

Tallima, H, and Ridi, RE (2018). Arachidonic acid: Physiological roles and potential health benefits – A review. Journal of Advanced Research 11, 33–41.

Tikhonova, IG (2016). Application of GPCR structures for modelling of free fatty acid receptors. In: Handbook of Experimental Pharmacology, 57–77.

Van Der Kant, R, Langness, VF, Herrera, C, Williams, DA, Fong, L, Leestemaker, Y, Steenvoorden, E, Rynearson, KD, Brouwers, JF, Helms, JB, *et al.* (2019). Cholesterol Metabolism Is a Druggable Axis that Independently Regulates Tau and Amyloid-β in iPSC-Derived Alzheimer's Disease Neurons. Cell Stem Cell 24, 363-375.e9.

Wang, B, Wu, L, Chen, J, Dong, L, Chen, C, Wen, Z, Hu, J, Fleming, I, and Wang, DW (2021). Metabolism pathways of arachidonic acids: mechanisms and potential therapeutic targets. Signal Transduction and Targeted Therapy 6.

West, AV, Muncipinto, G, Wu, H, Huang, A, Labenski, M, Jones, LH, and Woo, CM (2021). Labeling Preferences of Diazirines with Protein Biomolecules. Journal of the American Chemical Society 143, 6691–6700.

Wortmann, SB, Espeel, M, Almeida, LS, Reimer, A, Bosboom, D, Roels, F, De Brouwer, APM, and Wevers, RA (2014). Inborn errors of metabolism in the biosynthesis and remodelling of phospholipids. Journal of Inherited Metabolic Disease 38, 99–110.

Wymann, MP, and Schneiter, R (2008). Lipid signalling in disease. Nature Reviews Molecular Cell Biology 9, 162–176.

Xia, Y, and Peng, L (2013). Photoactivatable lipid probes for studying biomembranes by photoaffinity labeling. Chemical Reviews 113, 7880–7929.

Xu, S, and Tang, C (2022). Cholesterol and hedgehog signaling: mutual regulation and beyond. Frontiers in Cell and Developmental Biology 10.

Yu, C, Kennedy, NJ, Chang, CCY, and Rothblatt, J (1996). Molecular Cloning and Characterization of Two Isoforms of Saccharomyces cerevisiae Acyl-CoA:Sterol Acyltransferase. Journal of Biological Chemistry 271, 24157–24163.

Yue, S, Liu, J-J, Lee, SY, Lee, HJ, Shao, T, Song, B, Liu, C, Masterson, TA, Liu, X, Ratliff, TL, *et al.* (2014). Cholesteryl ester accumulation induced by PTEN loss and PI3K/AKT activation underlies human prostate cancer aggressiveness. Cell Metabolism 19, 393–406.

Zhang, J, Kelley, KL, Marshall, SM, Davis, M, Wilson, MD, Sawyer, JK, Farese, RV, Brown, JM, and Rudel, LL (2012). Tissue-specific knockouts of ACAT2 reveal that intestinal depletion is sufficient to prevent diet-induced cholesterol accumulation in the liver and blood. Journal of Lipid Research 53, 1144–1152.

Zhao, B, Song, J, and Ghosh, S (2008). Hepatic overexpression of cholesteryl ester hydrolase enhances cholesterol elimination and in vivo reverse cholesterol transport. Journal of Lipid Research 49, 2212–2217.

Supplementary

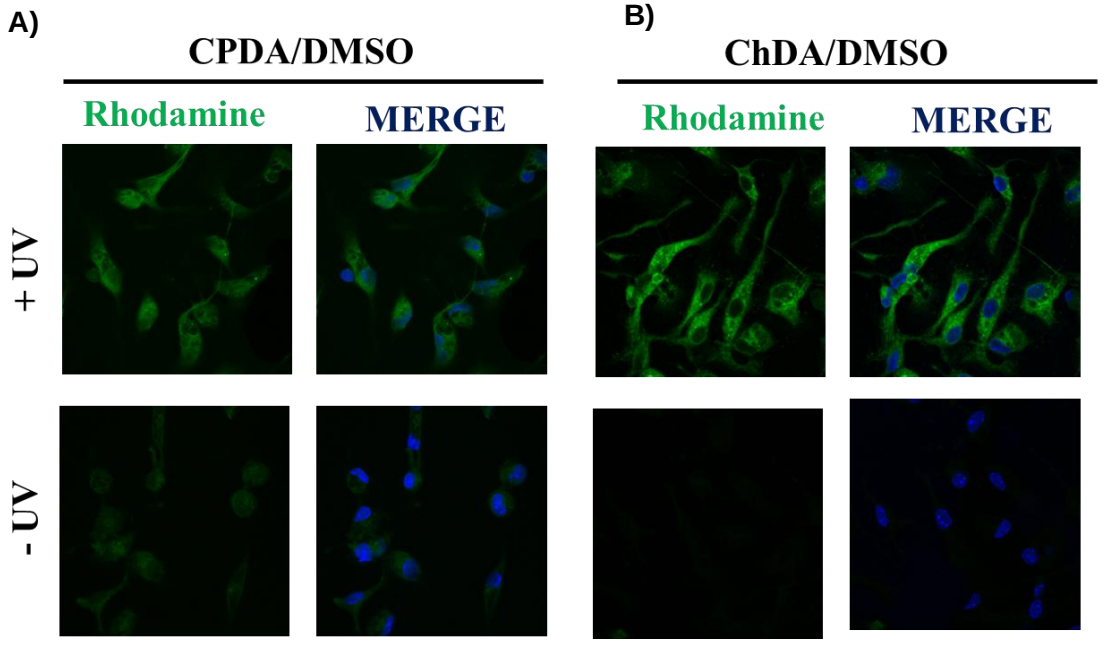

Figure S1. Visualising the probes in primary macrophages. A) with CPDA (in DMSO) B) with ChDA (in DMSO)

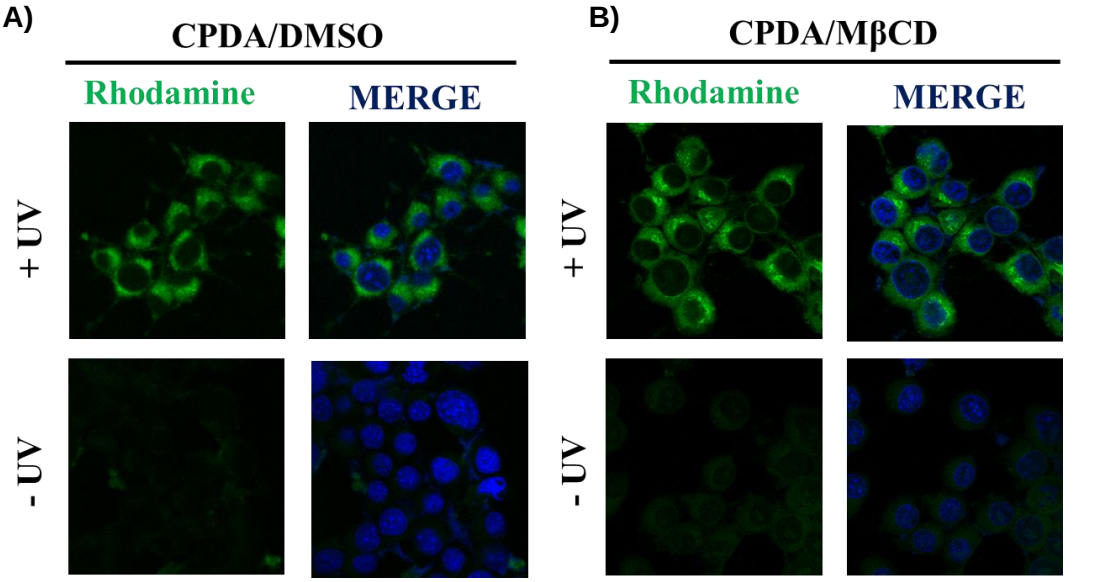

Figure S2. Visualising CPDA probes in N2a cell line. A) in DMSO and B) in MβCD

A)

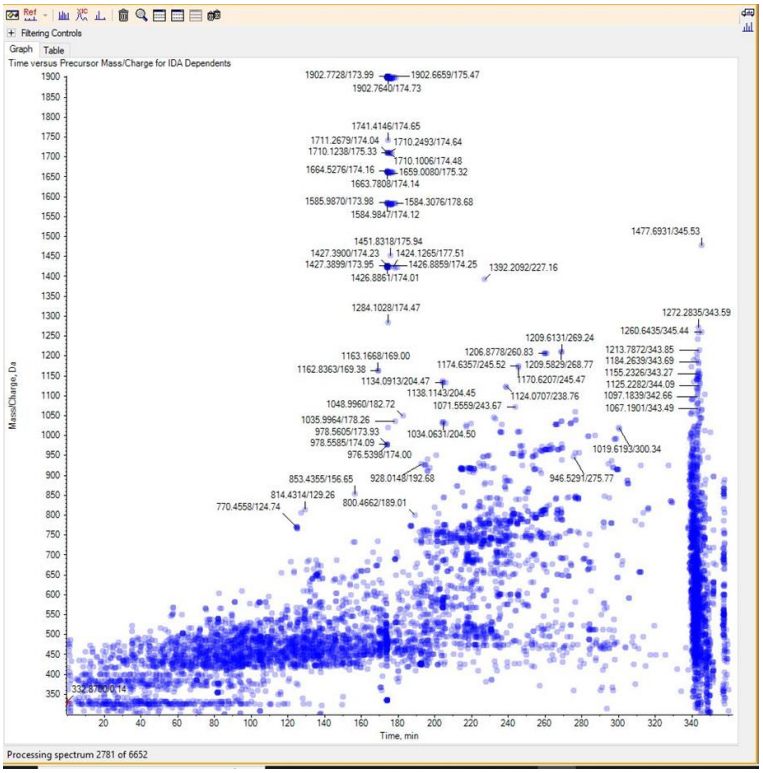

B)

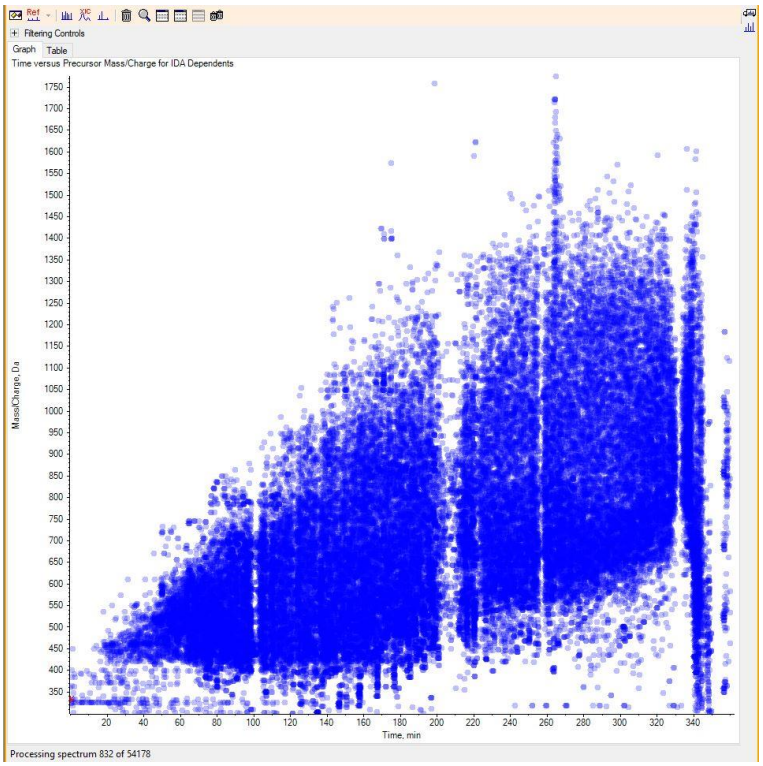

Figure S3. Representative spectral counts for proteomics A) Lower spectra obtained during initial attempts when protein concentration of 0.5 mg/mL was used (around 6600 counts) B) Higher spectra obtained when 1 mg/mL protein was used along with increased bead incubation time (around 54000 counts)